NAVAL POSTGRADUATE SCHOOL
Monterey, California

19980102 039

THESIS

**FREE ELECTRON LASER WEAPONS AND
ELECTRON BEAM TRANSPORT**

by

Rick A. Restivo

June 1997

Thesis Advisors: William B. Colson
                                    Robert L. Armstead

Approved for public release; distribution is unlimited.

REPORT DOCUMENTATION PAGE

Form Approved OMB No. 0704-0188

1. AGENCY USE ONLY *(Leave blank)*	2. REPORT DATE June 1997	3. REPORT TYPE AND DATES COVERED Master's Thesis

4. TITLE AND SUBTITLE FREE ELECTRON LASER WEAPONS AND ELECTRON BEAM TRANSPORT	5. FUNDING NUMBERS
6. AUTHOR(S) Restivo, Rick A.	

7. PERFORMING ORGANIZATION NAME(S) AND ADDRESS(ES) Naval Postgraduate School Monterey CA 93943-5000	8. PERFORMING ORGANIZATION REPORT NUMBER
9. SPONSORING/MONITORING AGENCY NAME(S) AND ADDRESS(ES)	10. SPONSORING/MONITORING AGENCY REPORT NUMBER

11. SUPPLEMENTARY NOTES The views expressed in this thesis are those of the author and do not reflect the official policy or position of the Department of Defense or the U.S. Government.

12a. DISTRIBUTION/AVAILABILITY STATEMENT Approved for public release; distribution is unlimited.	12b. DISTRIBUTION CODE

13. ABSTRACT *(maximum 200 words)*

The Navy is exploring the possibility of using a MW class free electron laser (FEL) as a ship self-defense weapon against anti-ship missiles. The Navy has helped fund the construction of a KW average power FEL and has held workshops to discuss weapons class FELs.

A design workshop resulted in two possible MW FELs which are examined. One of these designs, the MW regenerative amplifier FEL, is looked at further to determine the feasibility of its design parameters. The second design, the MW oscillator FEL, presents a challenge in understanding the electron beam transport phenomena known as coherent synchrotron radiation (CSR). A workshop concluded that CSR is potentially disruptive in the electron beam recovery in the oscillator design. Possible CSR experiments are analyzed to help the Nay's Directed Energy office determine which, if any, CSR experiment will be useful.

14. SUBJECT TERMS: Free electron laser, ship self-defense, coherent synchrotron radiation.			15. NUMBER OF PAGES 71
			16. PRICE CODE

17. SECURITY CLASSIFICATION OF REPORT Unclassified	18. SECURITY CLASSIFICATION OF THIS PAGE Unclassified	19. SECURITY CLASSIFICATION OF ABSTRACT Unclassified	20. LIMITATION OF ABSTRACT UL

FREE ELECTRON LASER WEAPONS AND ELECTRON BEAM TRANSPORT

Rick A. Restivo
Lieutenant, United States Navy
B.S., Texas A&M University, 1991

Submitted in partial fulfillment of the
requirements for the degree of

MASTER OF SCIENCE IN PHYSICS

from the

**NAVAL POSTGRADUATE SCHOOL
June 1997**

Author: _____

Rick A. Restivo

Approved by: _____

William B. Colson, Thesis Advisor

_____

Robert L. Armstead, Thesis Advisor

_____

Anthony A. Atchley, Chair, Department of Physics

ABSTRACT

The Navy is exploring the possibility of using a MW class free electron laser (FEL) as a ship self-defense weapon against anti-ship missiles. The Navy has helped fund the construction of a KW average power FEL and has held workshops to discuss weapons class FELs.

A design workshop resulted in two possible MW FELs which are examined. One of these designs, the MW regenerative amplifier FEL, is looked at further to determine the feasibility of its design parameters. The second design, the MW oscillator FEL, presents a challenge in understanding the electron beam transport phenomena known as coherent synchrotron radiation (CSR). A workshop concluded that CSR is potentially disruptive in the electron beam recovery in the oscillator design. Possible CSR experiments are analyzed to help the Navy's Directed Energy office determine which, if any, CSR experiment will be useful.

TABLE OF CONTENTS

ACKNOWLEDGEMENT

The author wishes to acknowledge the support of this research by the Naval Postgraduate School, the High Energy Laser office at the Space and Naval Warfare Command (SPAWAR), Thomas Jefferson National Accelerator Facility, Northrop Grumman Corporation, Boeing, Los Alamos National Lab, and Duke University.

I want to thank my thesis advisors, Professor Bill Colson and Professor Robert Armstead, for their many hours of assistance. I want to especially thank Professor Colson for teaching me about FELs and for his patience and sense of humor. Thanks also goes out to Dr. Robert Wong for his help with the UNIX system and to Dr. Doug Small for his countless tutoring sessions.

I want to thank my wife, Laure, for helping me in so many ways. Her sacrifices enabled me to complete this thesis and obtain a degree. Once again Laure, you are correct, the answer is 2.

I. INTRODUCTION

The first free electron laser (FEL) was demonstrated in 1976 by Madey and his co-workers at Stanford University [Ref. 1]. Since this time, scientists from around the world have worked to develop the field of FELs both experimentally and theoretically.

FELs have become an interest of the United States Navy as a possible solution to an important current problem. One of the most real and dangerous threats to Naval ships is anti-ship missiles (ASM) which are included in the arsenals of most every country in the world. With the increasing mission of single-ship operations and operations close to land masses world wide, each US Navy ship needs to be able to defend itself against a sudden ASM attack. The current close-in-weapon-system installed aboard ships is the Phalanx gun. This weapon is inadequate for protecting the ship against incoming missiles because the missile approaches too close to the ship before being destroyed by the gun. As a result, the Navy is exploring different options for a solution to this problem.

The advantage of lasers is the speed of propagation of the destructive energy, the speed of light, and the ability to focus intense energy to a small spot at 5 km to 10 km. These characteristics can increase the distance at which incoming missiles are destroyed, lessening the likelyhood of high energy debris impacting the ship. The flexibility of FELs has resulted in Navy funding to develop a MW FEL. Missiles require about 20 kW/cm^2 over 100 cm^2 to crack the structure which causes a rapid self destruction of the high speed missile. Therefore, a MW laser seems to be the range of power output suitable for this endeavor.

Currently, a 1 KW FEL is being constructed at Thomas Jefferson National Accelerator Facility (TJNAF) in Newport News, VA. This FEL will be the most powerful ever constructed. For this reason, the Navy's directed energy office is assisting in it's development to gain knowledge on high power FELs and their feasibility for a ship self-defense weapon system.

In hopes of developing a feasible design, the Navy assembled scientists from around the country for a 3 day MW FEL design meeting at TJNAF in September 1996. From the many designs presented, two FEL weapon designs emerged. These two designs, the MW regenerative amplifier design and the MW oscillator design, are reviewed and their strengths and weaknesses discussed.

Some analysis of each design determines the possible feasibility of these proposed FEL weapons. Analysis through computer simulations is conducted to evaluate the current parameters of the MW regenerative amplifier. A potential problem with the MW oscillator design stems from coherent synchrotron radiation (CSR) and its effect on emittance of the electron beam. This problem is reviewed along with the conclusions of an electron beam transport workshop held at NPS. Possible CSR experiments and parameters are listed and a relative comparison is made. One possible experiment involving the Princeton FEL (CIRFEL) is discussed and some computer analysis is conducted. This work is intended to aid the Navy's Directed Energy Office in its quest for a ship self defense FEL weapon.

II. BACKGROUND

A.   THE BASIC FREE ELECTRON LASER

An FEL uses a relativistic beam of electrons to generate electromagnetic radiation. A transverse, periodic magnetic field, called an "undulator", wiggles the electrons causing acceleration when the electrons experience Lorentz forces in the undulator as shown in Figure 1.
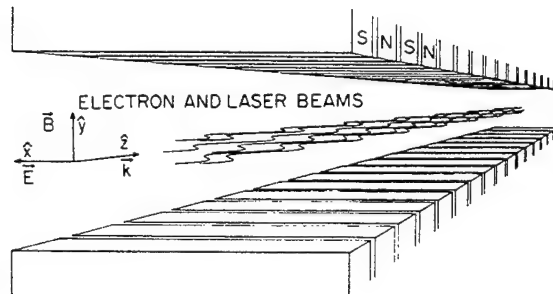
Figure 1. This is a typical undulator. The magnetic field
causes the electrons to wiggle in the transverse plane.
From Ref. [1].

The result is an interaction between the electron beam and the co-propagating electromagnetic wave and is the basic operating principle of all FELs. [Ref. 1]

The basic components of an FEL are an electron accelerator and an undulator. There are two distinct FEL designs: the oscillator and the amplifier. The oscillator has an optical cavity enclosed by mirrors with the undulator at the mid-section as shown in Figure 2. The oscillator transfers a small percentage of energy from the electron beam to the light wave on each successive pass of the oscillating light wave in the undulator.
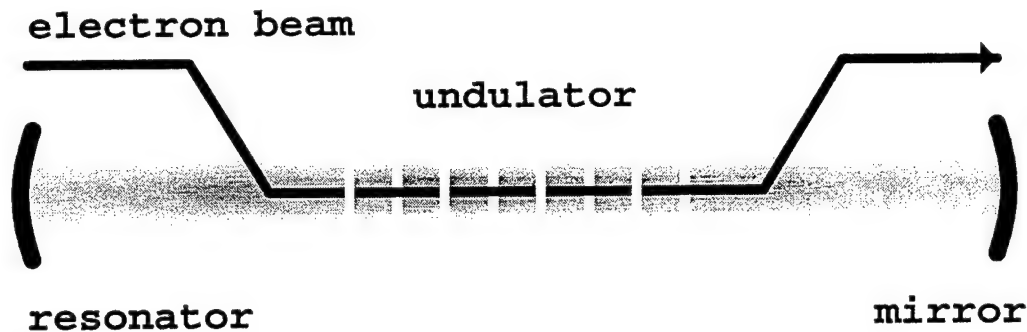
Figure 2. This is a typical FEL oscillator. The electron beam passes through the cavity and is acted on by the magnetic field from the undulator. Light is represented by the shaded portion between the two curved mirrors. From Ref. [2].

The amplifier looks similar but lacks the mirrors. The amplifier relies on a high percentage of the electron beam energy being transferred to the light wave on a single pass through the undulator. Typically, the oscillator will be designed to have low single-pass gain and the amplifier will have high gain.

Many parameters common to all free electron lasers have typical values. The distance from the center of one magnet to the center of the next magnet is defined as the undulator wavelength, λ_0, which varies from 2 cm to 10 cm. The number of periods, N, in undulators varies from 20 to several hundred. Since the length of an undulator is $L = N\lambda_0$, undulators range in length from 1 m up to 20 m. Electron beams used in FELs have radii, r_b, from a fraction of a mm up to a cm. Peak currents vary widely in FELs. Some peak currents are around 1 A and some are as high as a kA. The average current is much lower and has nominal values in the nA to mA range. One of the most desirable attributes of FELs is that they can be designed to

provide light at specific wavelengths, λ. The optical wavelengths of FELs range from $\lambda \approx 1$ cm to $\lambda \approx 200$ nm.

B. FREE ELECTRON LASER THEORY

1. The Pendulum Equation

The electrons traveling through the undulator experience forces from both the optical and undulator fields. By examining the electron dynamics classically, it can be shown that the equation which governs the electron's microscopic motion is the well-known equation describing the motion of a classical pendulum. This surprising parallel is extremely helpful in the understanding of free electron lasers. What follows is a derivation of FEL microscopic electron dynamics. [Ref. 3]

An important relation in FEL dynamics is the resonance condition. Light traveling at speed c overtakes electrons traveling at speed $\beta_z c$ in the undulator, where $\beta_z = v_z/c$, and v_z is the longitudinal speed of the electron. The definition of resonance is when one wavelength of light λ passes over an electron as the electron travels through one undulator wavelength λ_0. The time it takes an electron to travel through one undulator period is $t = \lambda_0/v_z = \lambda_0/(\beta_z c)$. After one undulator period, the one wavelength of light will be ahead of the electron a distance λ, where $\lambda = ct - v_z t = ct(1-\beta_z)$. Substituting for time gives the resonance condition,

$$\lambda = \lambda_0 \frac{1 - \beta_z}{\beta_z} \quad . \tag{1}$$

For highly relativistic electrons, as in an FEL, $\beta_z \approx 1$. In this case, the wavelength of the light will be much less than an undulator wavelength, $\lambda \ll \lambda_0$.

A static helical field from the undulator magnets takes the form

$$\vec{B}_u = B(\hat{i}\cos k_0 z + \hat{j}\sin k_0 z) \quad , \tag{2}$$

5

where $k_0 = 2\pi/\lambda_0$, and z is the longitudinal position along the undulator. The undulator wave number is k_0 and λ_0 is the undulator wavelength. B is the amplitude of the undulator magnetic field and $\hat{i}$, $\hat{j}$, and $\hat{k}$, are unit vectors in the x, y, and z directions respectively, as represented in Figure 1. (Note that the field in Figure 1 represents a linear undulator, not one that is helical.) The magnetic field strength for undulators is typically 2 to 7 kG. A circularly-polarized plane-wave is assumed for the optical field,

$$\vec{E}_o = E(\hat{i}\cos\psi - \hat{j}\sin\psi) \ , \ \vec{B}_o = E(\hat{i}\sin\psi + \hat{j}\cos\psi) \ , \tag{3}$$

where $\psi = kz - \omega t + \phi$, and $k = \omega/c$. The electric and magnetic field amplitudes are E, k is the optical wave number, ω is the angular frequency of the optical wave, c is the speed of light in vacuum, t is time, and ϕ is the optical phase.

The Lorentz force equations are,

$$\frac{d\vec{p}}{dt} = -e\left[\vec{E} + \vec{\beta} \times \vec{B}\right] \ , \ \frac{d(\gamma mc^2)}{dt} = -e \ \vec{v} \cdot \vec{E} \ , \tag{4}$$

where the electron velocity is $\vec{v} = \vec{\beta}c$, and the Lorentz factor is $\gamma = (1 - \beta^2)^{-\frac{1}{2}}$. The electron momentum is $\vec{p} = \gamma m\vec{v}$, the electron energy is γmc^2, m is the mass of an electron, and e is the electron charge magnitude [Ref. 4]. The electron energy in FELs ranges from a few MeV with $\gamma{\sim}5$ all the way to a few GeV with $\gamma{\sim}5000$. Substituting for the momentum in the Lorentz equations gives,

$$\frac{d\gamma\vec{\beta}}{dt} = -\frac{e}{mc}\left[\vec{E}_o + \vec{\beta} \times \vec{B}\right] \ , \ \frac{d\gamma}{dt} = -\frac{e}{mc}\left[\vec{\beta} \cdot \vec{E}_o\right] \ , \tag{5}$$

where $\vec{B} = \vec{B}_u + \vec{B}_o$.

The electric and magnetic fields, (2) and (3), are then inserted into (5) to yield,

$$\frac{d(\gamma\vec{\beta}_\perp)}{dt} = -\frac{e}{mc}\left[E(1-\beta_z)(\hat{i}\cos\psi - \hat{j}\sin\psi) + B\beta_z(-\hat{i}\sin k_0 z + \hat{j}\cos k_0 z)\right] \ , \tag{6}$$

$$\frac{d(\gamma\vec{\beta}_z)}{dt} = -\frac{e}{mc}\left[E(\beta_x\cos\psi - \beta_y\sin\psi) + B(\beta_x\sin k_0 z - \beta_y\cos k_0 z)\right]\hat{k} \ , \tag{7}$$

$$\frac{d\gamma}{dt} = -\frac{e}{mc}E\left[\beta_x\cos\psi - \beta_y\sin\psi\right] \ , \tag{8}$$

6

where $\vec{\beta}_\perp = \beta_x \hat{i} + \beta_y \hat{j}$, and $\vec{\beta}_z = \beta_z \hat{k}$. It is assumed that for relativistic electrons where $\beta_z \approx 1$, $E(1 - \beta_z) \ll B\beta_z$, so the first term on the right-hand side of (6) is ignored and β_z is set equal to one in the second term.

Remembering that $z = ct$ very nearly and solving (6) for $\vec{\beta}_\perp$ gives $\beta_x = -(K/\gamma)\cos k_0 z$ and $\beta_y = -(K/\gamma)\sin k_0 z$, where the undulator parameter is $K = eB/(k_0 mc^2)$. From the typical FEL parameters, $K \approx 1$. Perfect injection into helical orbits is assumed so the constant of integration is zero. Substituting the result for $\vec{\beta}_\perp$ into (8) gives the following equation for the electrons,

$$\frac{d\gamma}{dt} = \dot{\gamma} = \frac{eKE}{\gamma mc}\cos(\zeta + \phi) \quad , \tag{9}$$

where the electron phase in the combined undulator and light fields is $\zeta = (k + k_0)z - \omega t$, and $d/dt = (\;\dot{}\;)$. Squaring the result for $\vec{\beta}_\perp$ gives $\beta_\perp^2 = K^2/\gamma^2$ which further yields $1/\gamma^2 = 1 - K^2/\gamma^2 - \beta_z^2$ from the definition of the Lorentz factor. Solving for β_z and substituting into (1) for highly relativistic electrons where $\gamma \gg 1$, the resonance condition becomes,

$$\lambda \approx \frac{\lambda_0(1 + K^2)}{2\gamma^2} \quad . \tag{10}$$

Now the resonance condition is in terms of the electron energy. [Ref. 5]

To examine ζ, take time at $t = 0$ so $\zeta(0) = (k+k_0)z_0 \approx (2\pi/\lambda)z_0$, where z_0 is the initial electron position. We know $\lambda \ll \lambda_0$ which also means that $k \gg k_0$. Changing the electron initial position by an amount ranging from zero to one wavelength of light causes ζ to vary between 0 and 2π. From (9), a change in ζ of π causes $\dot{\gamma}$, the rate of change in energy of the electrons, to reverse sign. Since the electron beam spans many wavelengths of light, the electrons are uniformly distributed throughout each wavelength. For this reason about half the electrons will gain energy and about half will lose energy. As electrons gain energy, their velocity increases while electrons that lose energy decrease in velocity. This leads to bunching of electrons. Since $\dot{\gamma} > 0$ for

7

about half the electrons and $\dot{\gamma} < 0$ for the rest, there does not seem to be an overall change in energy, and therefore no gain. Gain will be discussed in the next section.

The next step in finding the pendulum equation is to relate $\dot{\gamma}$ to $\dot{\beta}_z$ using $\gamma^{-2} = 1 - \beta^2 = 1 - \beta_z^2 - \beta_\perp^2$. The values of β_x and β_y found previously give $(1 + K^2)\gamma^{-2} = 1 - \beta_z^2$. Taking the time derivative of each side and rearranging gives,

$$\frac{\dot{\gamma}}{\gamma} = \frac{\gamma^2 \beta_z \dot{\beta}_z}{(1 + K^2)} \quad . \tag{11}$$

The final step in arriving at the pendulum equation is to relate $\dot{\gamma}$ obtained in (11) to $\dot{\zeta}$. Using the definition for ζ, the second derivative with respect to time is $\ddot{\zeta} = (k + k_0)c\dot{\beta}_z$. This can be substituted into (11) to yield a relation between $\dot{\gamma}$ and $\ddot{\zeta}$. Since free electron lasers use highly relativistic electrons, $\beta_z \approx 1$, and $k \gg k_0$ so that the relation becomes $\dot{\gamma}/\gamma \approx \gamma^2 \ddot{\zeta}/[\omega(1 + K^2)]$. Substituting the resonance condition (10) into the newest relation between $\dot{\gamma}$ and $\ddot{\zeta}$ yields $\dot{\gamma}/\gamma \approx \ddot{\zeta}/2\omega_0$. Finally, substituting in the value of $\dot{\gamma}$ in (9) gives the microscopic electron equation of motion as,

$$\ddot{\zeta} \approx \frac{2\omega_0 eKE}{\gamma^2 mc} \cos(\zeta + \phi) \quad . \tag{12}$$

Now the microscopic electron phase dynamics are in the form of the pendulum equation. [Ref. 3]

Dimensionless parameters are introduced to enhance the understanding of FELs. The first such parameter will represent time. For an average electron, the time it spends in the undulator is determined by the length of the undulator L and the speed of the electron v_0 such that $t = L/v_0$. Remembering that $\beta_0 = v_0/c$ then $t = L/\beta_0 c \approx L/c$ since, for highly relativistic electrons, $\beta_0 \approx 1$. Now the dimensionless time τ will be defined as $\tau \approx ct/L$.

Substituting this dimensionless time parameter into (12) yields,

$$\overset{\circ\circ}{\zeta} = |a|\cos(\zeta + \phi) \quad , \tag{13}$$

where $|a| = 4\pi NeKLE/(\gamma^2 mc^2)$, the number of undulator periods is $N = L/\lambda_0$, ($^\circ$)

8

represents differentiation with respect to τ, the dimensionless optical field is $a = |a|e^{i\phi}$, and $i = \sqrt{-1}$. Typical values of the dimensionless optical field amplitude are $|a| \ll \pi$ for weak optical fields and $|a| \geq \pi$ for strong optical fields. The assumptions that have been made are $\gamma \gg 1$ for highly relativistic electrons so that $\lambda_0 \gg \lambda$, and therefore $k \gg k_0$. Examination of (13) shows that for $-\pi/2 < (\zeta + \phi) < \pi/2$, the phase acceleration $\overset{\circ\circ}{\zeta}$ is greater than zero, and for $\pi/2 < (\zeta + \phi) < 3\pi/2$, it is less than zero. Electrons that begin their evolution along the undulator randomly spread in phase space from $-\pi/2$ to $3\pi/2$, begin to bunch at $(\zeta + \phi) \approx \pi/2$ because of the differences in phase acceleration between the electrons surrounding $\pi/2$.

As the electron beam and optical wave interaction evolves, the optical field strength passes from the weak field regime to strong fields. In weak optical fields $|a| \ll \pi$, bunching of electrons is very slight. In strong fields $|a| \geq \pi$, electron bunching occurs rapidly and the electrons begin to become trapped in closed phase-space orbits, the boundary of which is represented by the "separatrix." The bunched electrons that are trapped, after causing gain, then shift in phase to one which causes the electrons to begin to absorb energy from the optical field, the result of which is a decrease in the optical field gain. As the gain begins to diminish the laser is said to have reached saturation. Gain is explained in detail in section 3 of this chapter.

An example is seen in Figure 3 where the final positions of 3000 sample electrons are shown in phase space. The electron phase velocity ν, defined as $\nu = \overset{\circ}{\zeta}$, is plotted on the vertical axis, and electron phase ζ is plotted on the horizontal axis. The electrons' initial phase velocities are distributed in a Gaussian with standard deviation $\sigma_G = 1$ around $\nu_0 = 3$. A number of electrons are trapped in closed phase-space orbits inside the solid line representing the separatrix. This is typical of a low gain oscillator in strong optical fields near saturation. The gain is plotted at the upper-right on a logarithmic scale from the beginning to the end of the undulator represented by $\tau = 0$ to $\tau = 1$, respectively. Note that saturation has been reached, marked by the decrease in gain near $\tau = 1$. Strong optical fields are represented since the initial

9

optical field strength $a_0 = 20 \geq \pi$. The dimensionless current density $j = 10$ and the dimensionless energy spread $\sigma_G = 1$ are explained further in section 3 and 4,
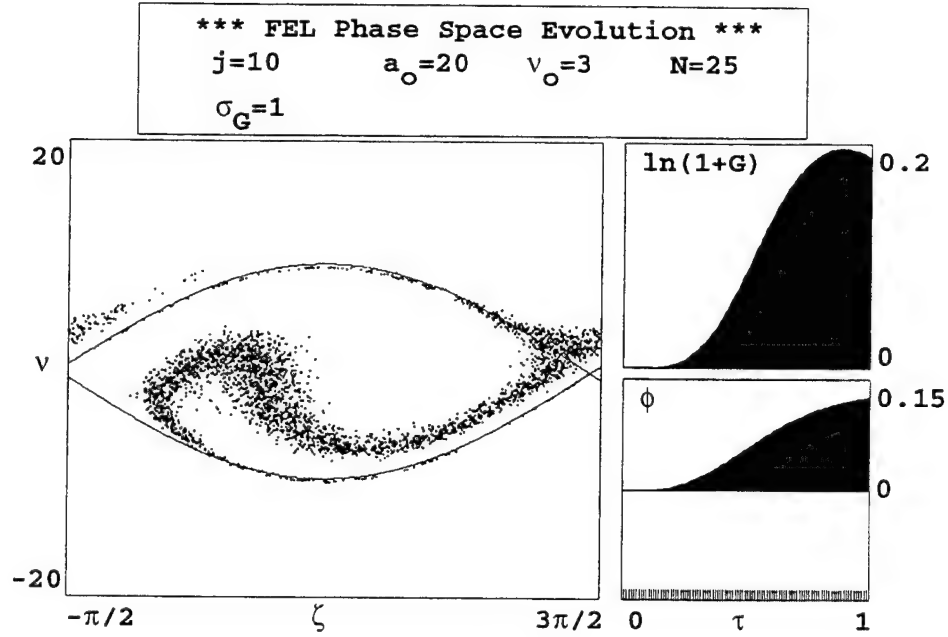
Figure 3. A plot of FEL phase space evolution for low gain.

respectively. There are $N = 25$ undulator periods and the optical phase is also shown in the lower-right portion of the figure. The optical phase is initially zero and steadily increases up to a final value of $\phi \approx 0.15$.

2.   The Optical Wave Equation

The pendulum equation, (13), governs the motion of the electrons in the undulator. The optical wave equation will now be developed so that the evolution of the complex radiation field can be described mathematically. The wave equation in a vacuum with no current density is of the form

$$\left[\vec{\nabla}^2 - \frac{1}{c^2}\frac{\partial^2}{\partial t^2}\right]\vec{A}(x,y,z,t) = 0 \tag{14}$$

where $\vec{\nabla} = \hat{i}\,\partial/\partial x + \hat{j}\,\partial/\partial y + \hat{k}\,\partial/\partial z$ and $\vec{A}$ is the vector potential from which $\vec{E}$ and $\vec{B}$ may be derived by $\vec{E} = (-1/c)\,\partial\vec{A}/\partial t$, and $\vec{B} = \vec{\nabla}\times\vec{A}$. A vector potential is selected in the form of a circularly polarized plane wave,

$$\vec{A} = \frac{E(\vec{x},t)}{k}[\hat{i}\sin\psi + \hat{j}\cos\psi]$$

where E is the complex electric field. The vector potential can be written in the following form

$$\vec{A} = \frac{\varepsilon}{k}\hat{e}e^{i(kz-\omega t)} , \tag{15}$$

where $\varepsilon = |E(\vec{x},t)|e^{i\phi(\vec{x},t)}$, ϕ represents the optical phase, and $\hat{e} = (-i,1,0)$ is the polarization vector. When evaluating (14) by substituting in (15), the slowly-varying amplitude and phase approximation is made. In this approximation, the field is taken to vary slowly in time during an optical period ($\dot{E} \ll \omega E$, $\dot{\phi} \ll \omega\phi$), and slowly in space over an optical wavelength ($E' \ll kE$, $\phi' \ll k\phi$) where ($'$) represents differentiation with respect to z. This is an appropriate assumption since an FEL emits a relatively narrow spectrum or linewidth. If the fields varied quickly, the emission spectrum would be broadband which is not the case. [Ref. 5]

Using $\varepsilon(x,y,z,t)$ and evaluating (14) by using (15), yields

$$\left[\frac{1}{2}\vec{\nabla}_\perp^2 + ik\left[\frac{\partial}{\partial z} + \frac{1}{c}\frac{\partial}{\partial t}\right]\right]\varepsilon(x,y,z,t) = 0 \tag{16}$$

where terms of $\ddot{\varepsilon}$ and ε'' have been ignored because of the slowly-varying amplitude and phase approximation, and $\vec{\nabla}_\perp = \hat{i}\,\partial/\partial x + \hat{j}\,\partial/\partial y$. The first term in (16) describes diffraction. A solution to the second term alone is of the form $\varepsilon = f(z-ct)$ where f represents any function. Using $\tau \approx ct/L$ and defining $\tilde{z} = z-ct$, it can be found that $\partial/\partial z + (1/c)\,\partial/\partial t = (1/L)\,\partial/\partial\tau$ where the $\tilde{z}$ terms have cancelled. In dimensionless parameters the optical field is represented by $a = |a|e^{i\phi}$ which is of the same form as

$\varepsilon = |E|e^{i\phi}$. The dimensionless optical field amplitude $|a| = 4\pi NeKL|E|/(\gamma^2 mc^2)$ includes the electric field amplitude. Exchanging ε for a, and including τ gives

$$\left[\frac{1}{2}\nabla_\perp^2 + \frac{ik}{L}\frac{\partial}{\partial\tau}\right]a = 0 \quad . \tag{17}$$

Again, the first term describes diffraction. If the two terms are comparable, then diffraction is important. If the first term is small in comparison with the second because the wave front is very wide, diffraction is not as important and can be ignored.

To obtain a completely dimensionless wave equation, two dimensionless terms are defined as $\tilde{x} = x\sqrt{k/(2L)}$ and $\tilde{y} = y\sqrt{k/(2L)}$. Using these terms $\vec{\nabla}_\perp^2 = (k/2L)\tilde{\nabla}_\perp^2$ where $\tilde{\nabla}_\perp^2 = \partial^2/\partial\tilde{x}^2 + \partial^2/\partial\tilde{y}^2$. Using this in (17) gives the dimensionless parabolic wave equation

$$\left[-\frac{i}{4}\tilde{\nabla}_\perp^2 + \frac{\partial}{\partial\tau}\right]a = 0 \quad . \tag{18}$$

This derivation began assuming no current density was present. In an FEL with an electron beam (18) becomes

$$\left[-\frac{i}{4}\tilde{\nabla}_\perp^2 + \frac{\partial}{\partial\tau}\right]a = -j\langle e^{-i\zeta}\rangle \tag{19}$$

where $\zeta = (k + k_0)z - \omega t$ is the electron phase in the combined undulator and light fields, and j is the dimensionless current density, $j = 8N(e\pi KL)^2\rho/(\gamma^3 mc^2)$ described in detail in the next section on gain [Ref. 5]. Values of j vary a great deal from one FEL to another with an approximate range from unity to several thousand.

In an oscillator FEL, the curvature of the resonator mirrors and diffraction play important roles in determining the shape of the optical mode. Spherical mirrors with $j = 0$ give rise to Gaussian optical modes and the solution to (19) is called a "Gaussian" beam because of the optical mode's transverse shape. This solution with $j = 0$ is

12

$$a_G(r,\tau) = \frac{a_0}{w(\tau)} e^{\left[\frac{-r^2}{w^2(\tau)z_0} + i\phi_G(\tau)\right]} \quad, \tag{20}$$

and

$$\phi_G(\tau) = -\tan^{-1}\left[\frac{\tau - \tau_w}{z_0}\right] + \frac{r^2(\tau - \tau_w)}{z_0^2 + (\tau - \tau_w)^2} \quad,$$

where $w^2(\tau) = 1 + (\tau - \tau_w)^2/z_0^2$, $r = (x^2 + y^2)^{1/2}$ is the radial coordinate, z_0 is the dimensionless Rayleigh length, $\phi_G(\tau)$ is the phase shift of the Gaussian mode, and τ_w is the position in τ of the optical mode waist. For example, if $\tau_w = 0.5$ then the optical mode waist is located at the midpoint of the undulator. The Rayleigh length is given by $\pi w_0^2/\lambda$ where w_0 is the size of the optical mode waist. The Rayleigh length is the distance in which the initial optical mode area doubles in size. The dimensionless Rayleigh length is then defined as $z_0 = \pi w_0^2/(L\lambda)$. This Gaussian beam represents an optical mode which contracts in the middle and expands at the ends and depends on the spacing and curvature of the mirrors. If the optical mode is a Gaussian, the initial phase velocity that yields resonance is shifted to $\nu_0 \approx 1/z_0$ instead of $\nu_0 = 0$ when z_0 is large. [Ref. 6]

In some cases, diffraction may not be important so that (19) simplifies to

$$\overset{\circ}{a} = -j<e^{-i\zeta}> \quad . \tag{21}$$

Now that the equations which govern the electron dynamics (13) and the optical wave (19) have been developed, the evolution of how the optical fields grow will be discussed.

3. The Gain Equations

FELs can be designed to have either low gain, as in a typical oscillator design, or high gain, as in a typical amplifier design. Gain is simply the fractional change in power of the optical field in a single pass through the undulator. From the conservation of energy, an energy change in the electron beam must result in an

13

opposite energy change in the optical field. The gain may be calculated using the change in energy of the electron beam divided by the optical wave energy.

The first step in in finding the average change in energy of the electron beam will be to find the change in energy of a single electron, $\Delta\gamma mc^2$. This change in energy will depend on the change in phase velocity of the electrons with respect to time. The phase velocity is defined as $v = \overset{\circ}{\zeta}$ and is $v = L[(k+k_0)\beta_z-k]$. Now a relation needs to be found between $\Delta\gamma$ and Δv. Remembering that $k \gg k_0$, then $\Delta v \approx Lk\Delta\beta_z$. Now using $N = L/\lambda_0$, $\lambda = 2\pi/k$, $\lambda_0 = 2\pi/k_0$, and (10) gives $\Delta v \approx N2\pi(2\gamma^2/(1+K^2))\Delta\beta_z$. Using (11), Δv gives,

$$\Delta v \approx 4\pi N\frac{\Delta\gamma}{\gamma} \ . \tag{22}$$

The change in energy of an electron becomes $\Delta\gamma mc^2 = \gamma mc^2\Delta v/(4\pi N)$.

The average change in energy of the electron beam, the change in phase velocity, Δv, is the difference between the average phase velocity, $<v>$, and the initial phase velocity, v_0, of the electrons, $\Delta v = <v> - v_0$. The relation $v = \overset{\circ}{\zeta}$ will be used to eventually obtain $<v>$. Using (13) in weak fields, ζ can be expanded in powers of the optical field a_0 so that $\zeta = \zeta^{(0)} + \zeta^{(1)} + \zeta^{(2)} + \cdots$. For the expansion, $a(0) = a_0$ and $v^{(0)} = v_0$. So now $\overset{\circ}{\zeta}{}^{(0)} = v_0$ and integrating with respect to τ will give $\zeta^{(0)} = v_0\tau + \zeta_0$. Now (13) will become $\overset{\circ\circ}{\zeta}{}^{(1)} = a_0\cos(\zeta^{(0)}) = a_0\cos(\zeta_0 + v_0\tau)$. Successive integrations will yield $\zeta^{(1)}$ so that

$$\zeta = \zeta_0 + v_0\tau - \frac{a_0}{v_0^2}\left[\cos(\zeta_0 + v_0\tau) - \cos(\zeta_0) + v_0\tau\sin(\zeta_0)\right] + \dots \ . \tag{23}$$

All the terms in the expansion of ζ can be found by repeating this sequence. To obtain v, only terms of $\zeta^{(0)}$, and terms of $\zeta^{(1)}$ to first order will be kept ignoring $(\zeta^{(1)})^2$ and higher order terms. Differentiating ζ gives

$$\nu = \nu^{(0)} + \nu^{(1)} + \nu^{(2)} + \ldots = \nu_0 + \frac{a_0}{\nu_0}\left[\sin(\zeta_0 + \nu_0\tau) - \sin(\zeta_0)\right] + \tag{24}$$

$$+ \frac{a_0^2}{\nu_0^3}\left[-\frac{1}{4}\left[\cos(2\zeta_0 + 2\nu_0\tau) - \cos(2\zeta_0)\right] + \cos(\nu_0\tau) - 1 - \nu_0\tau\sin(\zeta_0)\cos(\zeta_0 + \nu_0\tau)\right] + \ldots \quad .$$

The next step will be to obtain $\langle\nu\rangle$ from (24).

The average changes in phase velocity of an electron will be obtained by $(1/2\pi)\int_0^{2\pi} \nu d\zeta_0$. Using this to evaluate (24), the last term in (24) will be the only term to survive so that

$$\langle\nu\rangle = \langle\nu^{(2)}\rangle + \cdots = \frac{a_0^2}{2\nu_0^3}\left[2\cos(\nu_0\tau) - 2 + \nu_0\tau\sin(\nu_0\tau)\right] + \cdots \quad . \tag{25}$$

This relation will be used to find $\Delta\nu$ in (22). Now the average change in energy of an electron is

$$\Delta\gamma mc^2 \approx \frac{\gamma mc^2(\langle\nu\rangle - \nu_0)}{4\pi N} \quad . \tag{26}$$

Before introducing the gain equation for low gain, the "filling factor" F, will be introduced which is the area of the electron beam divided by the area of the optical beam, $F = r_b^2 / w_0^2$, where r_b is the radius of the electron beam and w_0 is the optical beam waist. This factor arises because only a fraction of the optical mode is filled with electrons and accounts for the fraction of the two beams which interact with each other and therefore affect the gain. Now the average change in energy of the entire electron beam will be $(\rho F dV)(\Delta\gamma mc^2)$ where ρ is the electron density and dV is the volume occupied by the optical mode one wavelength of light long. A typical value of $\rho \approx 10^{12}$ cm^{-3} for a current of $I = 100$ A and $r_b \approx 1$ mm. [Ref. 7]

The radiation energy contained in a volume dV is $2E^2dV/8\pi$ [Ref. 7], so the gain equation is

$$G = -\frac{[\rho F dV][\gamma mc^2(\langle\nu\rangle - \nu_0)/(4\pi N)]}{2E^2 dV/8\pi} \quad . \tag{27}$$

15

This equation is true only for low gain since a_0 has been held fixed when interpreting (23) and (24). In weak optical fields, ζ can be expanded to obtain $<v>$, substituting (25) into (27) and simplifying yields the following equation for low gain in weak fields,

$$G = j \ \frac{[\ 2 - 2\cos(v_0\tau) - v_0\tau\sin(v_0\tau)]}{v_0^3} \ .$$

(28)

In (28), $j = 8N(e\pi KL)^2\rho F/(\gamma^3 mc^2)$ is the dimensionless current density, and is the most important FEL parameter. Low gain corresponds to $j \leq \pi$ and high gain corresponds to $j \gg \pi$.

An example of low gain in weak fields is shown in Figure 4. The figure shows the final gain spectrum $G(v_0)$ at $\tau = 1$, the end of the undulator, plotted against the


```
**** Gain Curve ****
j=1        a =0.01        N=25
            o
     Maximum gain at v = 2.6
                       o
```

Gain   0.13

                                        0.0

                                        -0.13

-12   v   12
                        o

Figure 4. The gain spectrum $G(v_0)$ for low current and weak fields.

initial phase velocity v_0. The dimensionless current density $j = 1 \leq \pi$ is in the low gain regime and the initial optical field strength $a_0 = 0.01 \ll \pi$ represents a weak field. There are $N = 25$ undulator periods with a maximum gain of $G = 0.13$ at phase velocity $v_0 = 2.6$. The gain is anti-symmetric about the resonance $v_0 = 0$, and positive

16

gain occurs for $v_0 > 0$. For $v_0 < 0$ the gain is negative which means the electron beam is absorbing energy from the optical wave. A shift in $v_0 \approx 2\pi$ can cause a shift from positive gain, amplification, to negative gain, absorption.

The development of the gain equation for large $j \gg \pi$ requires the use of the wave equation, because the optical field grows rapidly. The expansion performed to obtain the low gain equation cannot be used. For high gain, the governing equation is

$$G(\tau) \approx \frac{1}{9} e^{[(j/2)^{1/3} \sqrt{3} \tau]} \quad , \tag{29}$$

from [Ref. 8]. The gain is exponential in τ along the undulator with growth rate proportional to $j^{1/3}$. For high gain, the growth rate can be very high.

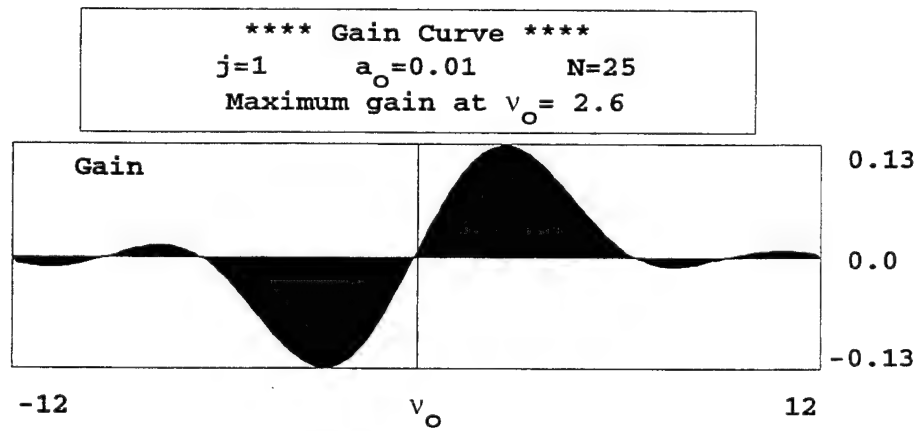An example of high gain in weak fields is shown in Figure 5. The figure shows the final gain spectrum $G(v_0)$ at $\tau = 1$, the end of the undulator, plotted against the initial phase velocity v_0. The dimensionless current density $j = 1000 \gg \pi$ is in the high-gain regime with $N = 200$ undulator periods which is typical of an FEL amplifier.
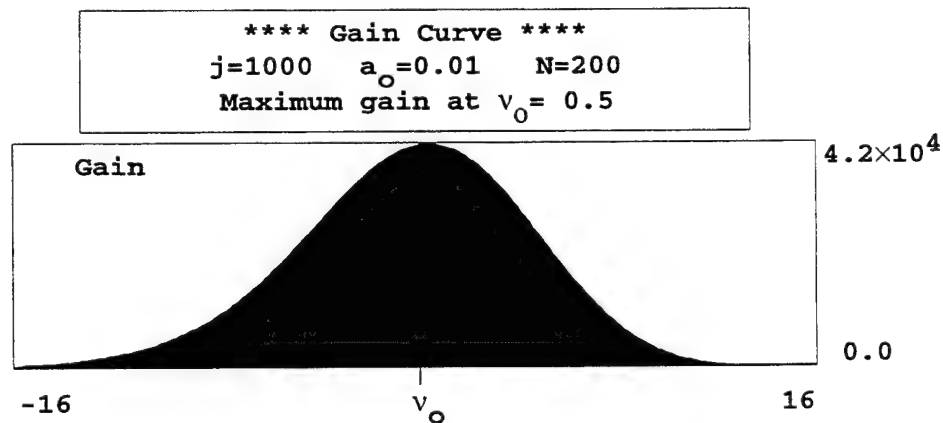

Figure 5. The gain spectrum $G(v_0)$ for high current and weak fields.

The maximum gain of $G = 4.2 \times 10^4$ occurs near resonance, $\nu_0 \approx 0$ and the gain spectrum is almost symmetric about resonance.

4.   Electron Beam Quality

One of the basic components of every FEL is some type of electron gun and accelerator. This initial production of electrons is important to the resulting output of the FEL. There is a tradeoff between high beam current and good beam quality; increasing beam current often comes at the expense of beam quality. The dimensionless current $j \propto IN^3$ where I is the actual current and N is the number of undulator periods, so increasing the number of undulator periods would be an approach to increasing j [Ref. 9]. However, an FEL with a longer undulator is more sensitive to beam quality than a shorter undulator because of the narrow gain spectrum bandwidth.

To represent the angular distribution of electrons about the z-axis, σ_θ is defined as

$$\sigma_\theta = \frac{2\pi N \gamma^2 \bar{\theta}^2}{1 + K^2} \tag{30}$$

where $\bar{\theta}$ is the root mean square (rms) injection angle of an electron. The distribution of the electrons in position is represented by

$$\sigma_e = \sqrt{\frac{\pi}{\lambda L}}\, r_0 \tag{31}$$

where r_0 is the rms distance of the electron from the z-axis. [Ref. 9]

A term commonly used to describe beam quality is emittance. The rms emittance is defined as $\varepsilon_{rms} = \pi \bar{\theta} r_0$. It turns out that the emittance is a constant along the length of the undulator [Ref. 10], so decreasing the electrons injection angle $\bar{\theta}$ results in an increased displacement from the z-axis, r_0. Using (30), (31), and (10) the definition of emittance becomes $\varepsilon_{rms} = \pi \lambda \varepsilon$ where

18

$$\varepsilon = \frac{\sigma_e \sqrt{\sigma_\theta}}{\pi} \tag{32}$$

is the dimensionless emittance. Another useful definition of emittance is normalized emittance defined as

$$\varepsilon_N = \gamma \varepsilon_{rms} \quad , \tag{33}$$

which is usually stated in units of π mm-mrad.

While emittance determines beam quality in the transverse direction, it does not correspond to the beam's longitudinal distribution. The term which describes this longitudinal spread is

$$\sigma_G = 4\pi N \frac{\Delta \gamma}{\gamma} \quad , \tag{34}$$

where $\Delta \gamma mc^2$ is the rms change in energy of an electron from the resonance energy [Ref. 9]. The longitudinal spread corresponds to an energy spread in the electrons.

Electrons do not all enter the undulator perfectly but are randomly distributed in both the longitudinal and transverse directions. A Gaussian distribution of the electrons is assumed of the form

$$f(x) = \frac{e^{-\frac{x^2}{2\sigma^2}}}{\sqrt{2\pi} \, \sigma} \tag{35}$$

where σ is the standard deviation and x is the parameter which is being distributed [Ref. 9]. An example of the effect of beam quality on an FEL is shown in Figure 6. As with Figure 3, this phase space evolution is generated by solving the pendulum equation (13) and the wave equation (21) numerically. The dimensionless current density $j = 10$ is at the low end of the high gain regime and strong fields are represented by the initial optical field strength $a_0 = 20 \geq \pi$. The initial phase velocity is $\nu_0 = 3$ with $N = 25$ undulator periods. The longitudinal energy spread $\sigma_G = 4$ is increased from $\sigma_G = 1$ in Figure 3. This degradation in beam quality causes less

19

bunching which is visible when comparing Figure 3 to Figure 6. The energy spread is responsible for a decrease in final gain to $G = 0.1$ and a smaller optical phase shift ϕ.
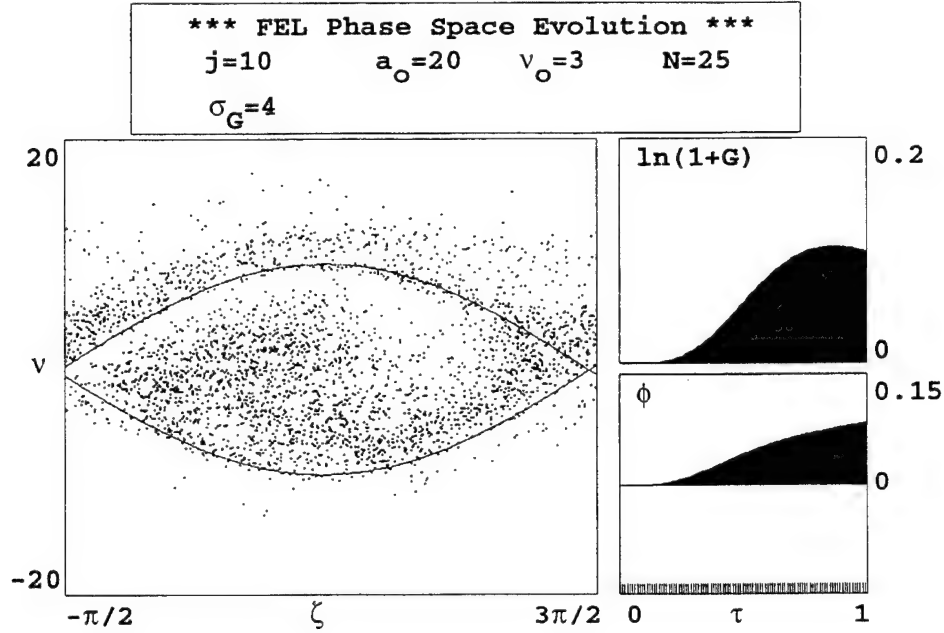
Figure 6. A plot of FEL phase space evolution for low gain with electron beam degradation.

While gain is the fractional increase in the optical field $|a|^2$, the FEL efficiency is the fraction of the electron beam energy extracted by the optical wave. The "natural" efficiency of an FEL as it reaches saturation is $\eta^* \approx 1/(2N)$. If N is increased to increase gain, the efficiency is decreased. Ultimately, the true efficiency of an FEL is simply the ratio of the power taken from the electron beam compared to the initial power in the electron beam. [Ref. 11]

5. The Tapered Undulator

As an FEL reaches saturation the electrons have given up enough energy so that they are no longer in resonance with the optical wave and gain decreases. Tapering an undulator changes the undulators' resonance condition along the length of the undulator so the electrons remain in resonance longer, hence increasing the overall gain in strong fields. Tapering can be done by decreasing the undulator wavelength λ_0 in the z-direction, or decreasing the magnetic field strength B, or both. Tapering essentially has the same result as accelerating the electrons. So, tapering acts as an artificial acceleration to the electrons. This artificial acceleration is represented by a dimensionless parameter δ. When λ_0 is decreased, this artificial acceleration is given by $\delta \approx -2\pi N \Delta\lambda_0/\lambda_0$ and when the undulator field strength is decreased it is given by $\delta \approx -4\pi N K^2 \Delta B/B(1+K^2)$. Some criteria for tapering must be met and are summed up in the following relations as

$$|a| > \delta \geq 4|a|^{1/2} \geq 2\pi \quad . \tag{36}$$

The tapered undulator is more efficient in strong optical fields than an untappered undulator. This is where the taper is designed to be effective. However, a tapered undulator has lower gain in weak optical fields than an untapered undulator. The efficiency of a tapered undulator is estimated by as $\eta_\delta \approx \delta/(8\pi N)$. For example, if $\delta \approx 20\pi$ and $N = 100$ periods, then $\eta_\delta \approx 5/(2N)$ while the natural efficiency is only $\eta^* \approx 1/(2N)$. So tapering, in this case, has increased the efficiency by a factor of 5. Tapering is a way to obtain higher overall gain in strong fields and higher efficiency. [Ref. 12]

An example of the tapered undulator in strong optical fields is shown in Figure 7. This example is based on a regenerative amplifier design developed by the FEL group at NPS and presented at the MW workshop September 24-26, 1996, in Newport News, VA. A regenerative amplifier FEL is basically the same as an amplifier FEL. The difference is that a regenerative amplifier takes approximately 1% to 10% of the

21

optical field (0.01% to 1.0% of the optical power) from the end of the undulator and feeds this back to the beginning of the undulator. The light that is fed back is focussed at the front of the undulator. This design is based on an undulator length L = 8 m, peak current of 600 A, and a goal for gain $G \geq 1000$. The dimensionless
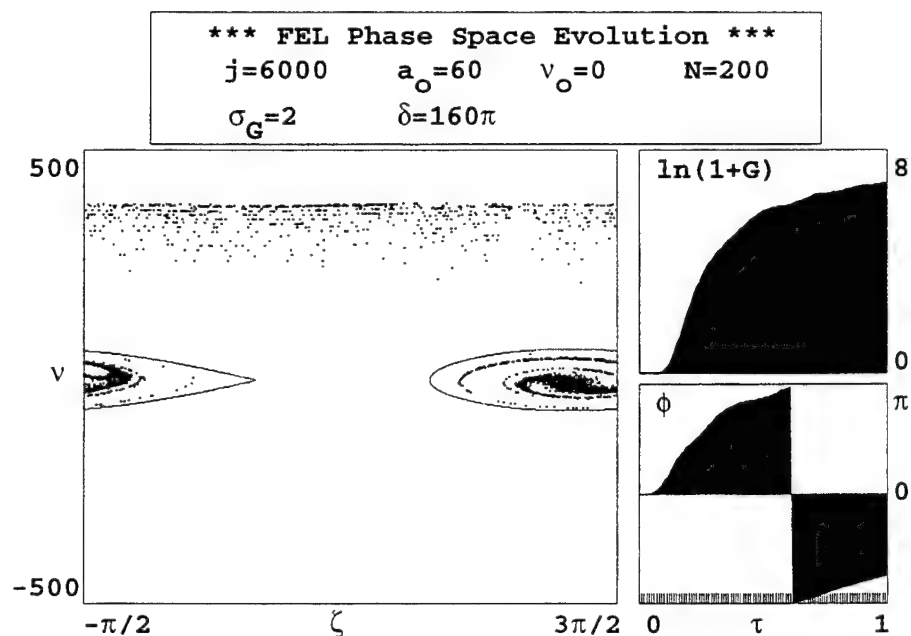
Figure 7. A plot of FEL phase space evolution for high gain in strong fields with a tapered undulator.

current density $j = 6000 \gg \pi$ is in the high gain regime and strong fields are represented by $a_0 = 60 \geq \pi$. As seen in Figure 5, the phase velocity for maximum gain occurs at resonance, $\nu_0 = 0$. The number of undulator periods, N = 200 is typical of an FEL amplifier and the Gaussian spread $\sigma_G = 2$ is nominal. The tapering parameter $\delta = 160\pi$ turns on at $\tau \approx 0.3$ and results in final gain of $G \approx 1000$ and extraction efficiency $\eta \approx 11\%$. Gain is roughly exponential from $\tau \approx 0.1$ to $\tau \approx 0.3$ where the taper turns on, and is represented by a straight line on the log plot. Saturation is then reached, but tapering allows gain to still increase slowly instead of

decreasing, after saturation, as in Figure 3. The trapped electrons are responsible for gain and are shown inside the separatrix. The untrapped electrons near $v \approx 400$ are shifted in phase velocity by the tapering whereas the trapped electrons remain near resonance because of strong fields. The optical phase shift $\Delta\phi \approx 1.5\pi$ over the length of the undulator is characteristic of high gain. This phase shift is plotted in the lower right-hand portion of the figure. A value of $\phi \geq \pi$ is represented by a negative value of phase. The actual value for ϕ in this example simply continues to grow from $\phi = \pi$ to $\phi \approx 1.5\pi$.

Normally, natural diffraction of light would cause the optical field to expand in the transverse direction over the long propagation length of this undulator. If this occurred, the electron beam would become uncoupled from the optical field and the FEL interaction would stop. High current density of the electron beam, as seen here, causes light to focus back down on the electron beam, hence counteracting diffraction. The phase shift imposed by diffraction is opposite to the phase shift resulting from the high current. This effect is termed optical guiding [Ref. 13]. The large optical phase shift in Figure 7 represents optical guiding which is an important part of a high gain, high current FEL.

III.   MW-CLASS FREE ELECTRON LASER

A.   FEL PARAMETERS

In order to destroy an incoming missile, the laser power required on the missile surface is about 2 kW/cm^2 over a $w_0 \approx 6$ cm radius spot for a 3 second duration. The extinction coefficient due to aerosols at sea level is $\alpha \approx 0.05$/km, and $e^{-\alpha z}$ estimates the power remaining at $\lambda \approx 1$ µm wavelength over a distance z. For an example, assume an oscillator FEL with $N = 25$ periods, a peak current $\hat{I} = 600$ A, a pulse duration of 3 ps, and a repetition frequency of 500 MHz. For $\lambda \approx 1$ µm with a nominal undulator period of $\lambda_0 = 4$ cm and an assumed undulator parameter $K = 1$, (10) yields an electron beam energy $\gamma mc^2 \approx 100$ MeV. The duty factor for this example is $D = (3 \text{ ps})(500 \text{ MHz}) = 0.0015$. The average current is $\bar{I} = D\hat{I} = 0.9$ A which is much higher than typical FELs. To calculate the laser power which must leave the ship's FEL to destroy the missile at a range of $z = 8$ km, the following steps are taken. The power required to destroy the missile is $P_d = 226$ kW. The relationship between the power leaving the ship and the power arriving at the missile is $P_d = P_{ship}e^{-\alpha z}$. Therefore, the laser power which must leave the ship is $P_{ship} = 338$ kW. The electron beam peak power is $\hat{P} = \hat{I}V = (600 \text{ A})(100 \text{ MeV}) = 60 \text{ } GW$ which gives an average electron beam power of $\bar{P} = \bar{I}V = 90$ MW. The efficiency necessary to destroy an ASM is $\eta = P_{ship}/\bar{P} = 0.004$. An approximation for the natural single-pass efficiency of an FEL is $\eta^* = 1/(2N) = 0.02$ which is better than the required efficiency. Therefore, this example gives the required power density to destroy a missile. This type of calculation is the main driving factor in determining the FEL parameters for a possible weapons class FEL.

B.   REVIEW OF MW WORKSHOP

One threat to all Navy ship's is an attack with an anti-ship missile (ASM). These weapons are part of the arsenal of many countries around the world, so the threat is real. These missiles are very fast and have a small radar cross section which makes them hard to detect. The Navy is performing more operations where a sole ship is sent to do a mission. An example is current anti-drug operations where a single ship operates close to shore for weeks at a time. Each ship must be capable of defending itself from ASM's. For these reasons, an ASM is not something a battle group can be expected to defend individual ships against. Today, almost every US Naval ship has one or more PHALANX guns on board, the purpose of which is to defend the ship against an ASM attack. This is an illustration of how real the ASM threat has become.

The current close-in-weapon-system (CIWS) weapon system has been tested against actual missiles. The author's opinion is the CIWS is very capable of destroying an ASM. However, there is still a major problem with the PHALANX gun. The ASM is destroyed at such a close range that most of the debris, and a significant amount of energy, strikes the ship [Ref. 14]. While this may or may not be better than the intact ASM striking the ship, the ship is ultimately damaged by the ASM, which is the intent of the enemy.

In an effort to replace this current weapon system, the Navy is exploring the use of an FEL as a ship self-defense (SSD) weapon. The range at which an ASM can be engaged increases from a few hundred meters to about 5-10 kilometers when a laser is used in place of the PHALANX gun. It has been estimated that it would take about 3 seconds for a laser beam to burn a hole in a missile cone. Because of the missile's high speed, this hole would cause the missile to self destruct as a result of the reduction of aerodynamic properties and the ensuing forces this causes. Even for a missile traveling at Mach 3, if it is engaged at 5 km it will only have closed to a

range of approximately 2 km after the 3 second duration. Consequently, an FEL would keep the ship from being damaged by the ASM, thereby defeating the enemy's attempt.

An FEL is of interest for many reasons. A high power laser, on the order of a MW, will be required to destroy an incoming ASM. It is believed by commercial industry and the scientific community that high average powers can be achieved with FELs. Any SSD laser system will have to propagate in a maritime atmosphere where there are certain windows of propagation available. Being able to design the laser weapon system to a very specific wavelength is advantageous. The optical wavelength λ of an FEL can be chosen by (10). If actual tests show that the desired wavelength is slightly different than originally believed, then modifying an FEL to adapt to the new wavelength is a relatively minor task. This ease of re-design is true for FELs but not for other lasers. For these reasons, the Navy is considering an FEL for ship self-defense.

Currently, an infrared kilowatt FEL is under construction at Thomas Jefferson National Accelerator Facility (TJNAF) in Newport News, VA. This project, which has military as well as industrial applications, seeks to prove that a high average power FEL is a real possibility. In April 1996, the KW FEL project was started with US Navy funding. The Navy believes this laser will provide the Navy and the scientific community enough knowledge to be able to advance the FEL technology into a compact weapon design for ship self-defense.

The Navy sponsored a MW class FEL concepts workshop at TJNAF on September 24-26, 1996. There were 57 attendees from government, national labs, universities, and industry. The tasking statement for this workshop was, "The workshop is to develop material for incorporation in a SSD FEL Systems Engineering Management Plan, and is to define baseline concepts and technology options for subsequent system performance and cost trades." [Ref. 15] While the Navy is not yet ready to construct a weapons class FEL, the meeting was designed to discuss the

feasibility of this idea, and to bring out some of the possible pitfalls which must be overcome. Out of the workshop came two possible designs which are discussed in the next section.

C.   WORKSHOP RESULTS

Two conceptual designs came from the workshop. One design is an oscillator and the other is an amplifier. While these are very different approaches to a weapons class FEL, both are proposed to achieve the same goal. The goal is to produce enough average power to propagate energy through the atmosphere and burn a hole in a missile 5 to 10 km away. These two basic FEL designs evolved from a culmination of ideas presented at the workshop.

The typical FEL oscillator design uses mirrors and small extraction efficiency to obtain the desired optical field strength. A simple schematic of the oscillator design is shown in Figure 8. The FEL depicted in Figure 8 has an overall length of 16.5 meters
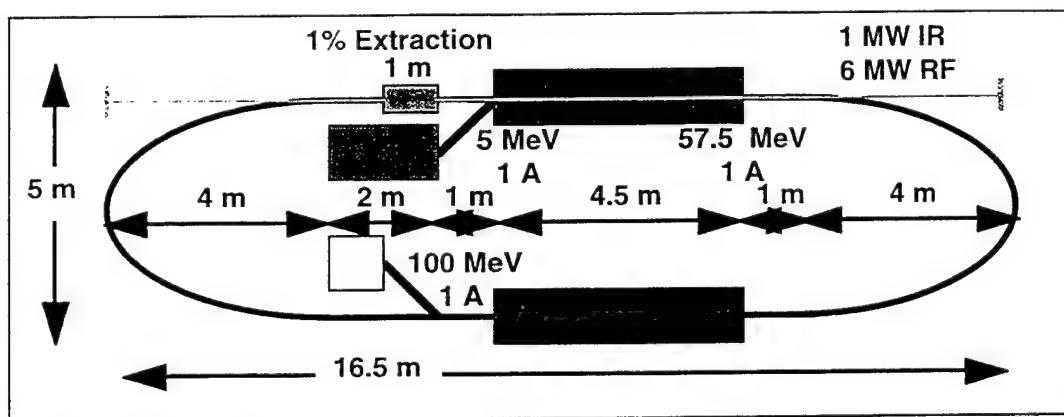

Figure 8. This is a conceptual MW class oscillator FEL.
From [Ref. 15].

28

and a width of 5 meters. A uniform undulator only 1 meter long is responsible for 1% extraction efficiency. One unique characteristic is the fact that this design makes use of energy recovery. This concept involves extracting energy from the $\gamma mc^2 = 100$ MeV electron beam in the undulator. Then, before sending the electrons to the beam dump, they are decelerated. This deceleration allows the energy, which would otherwise be dumped, to be partially recovered. In the process, the electrons travel around a race track vacuum chamber. The same accelerator is used to decelerate and recover most of the left over beam energy. The design in Figure 8 has an average current $\bar{I} = 1$ A. The input power is (1 A)(100 MeV) = 100 MW but 95 MW are recovered. With the output of 1 MW optical power this system requires a total input RF power of 6 MW.

In the oscillator, the optical field increases gradually as the light bounces between the cavity mirrors. The optical field reaches high power which requires the mirrors to withstand high power density on their surface. If the power density on the mirrors is too high, mirror damage will occur. The power density placed on the mirrors can be reduced by designing the oscillator FEL with a short Rayleigh length [Ref. 16]. Depending on the design, the mirrors may or may not be at risk.

An advantage of the oscillator design is that it appears to result in a more compact overall design. Space is critical on a ship so a smaller, but just as capable weapon, is a benefit. However, the overall volume of the oscillator and amplifier may be about the same.

The fact that the oscillator design relies on energy recovery brings about both advantages and disadvantages. Extracting energy from the electrons leads to a smaller beam dump. On a ship, disposing of high energy electrons can be a problem. Radiation is given off during deceleration. This radiation can be harmful to both personnel and equipment if the beam is above 15 MeV energy. Shielding people and equipment from this radiation involves adding weight to a ship which is a great concern. So, the lower the energy of the electron beam entering the beam dump, the

better. To date, energy recovery has never been performed. One of the goals of the infrared kilowatt FEL at TJNAF is to demonstrate energy recovery. Another potential problem which stems from energy recovery is having to transport the high energy electron beam around a bend with the energy spread imposed by the FEL interaction. Electron beam transport is the subject of Chapter V.

The regenerative amplifier design uses a longer undulator and relies on higher extraction efficiency to achieve high average power. A simple schematic of the regenerative amplifier design is shown in Figure 9. The FEL depicted in Figure 9 has
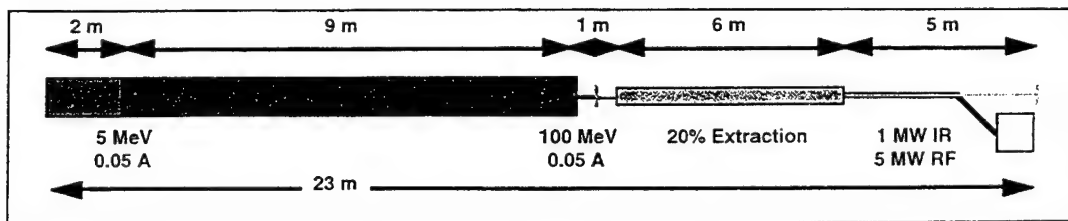
Figure 9. This is a conceptual MW class amplifier FEL.
From [Ref. 15].

an overall length of 23 meters. A 6 meter long undulator is used to achieve 20% extraction efficiency from the 100 MeV electron beam. The undulator is uniform during the first half and tapered during the second half in order to achieve the higher extraction efficiency. The regenerative amplifier uses mirrors to feedback a small amount of the optical beam power which is then focused at the beginning of the undulator. At the end of the system, the high energy electron beam is diverted to a beam dump. The design in Figure 9 has an average current $\bar{I} = 0.05$ A. This requires approximately 5 MW of input RF power and provides 1 MW of optical power in the infrared (IR) just as the oscillator design.

The amplifier design has advantages and disadvantages. This design does not use energy recovery so there is no requirement to bend the high energy beam. The bending may cause deterioration of the electron beam quality. Without energy recovery the electron beam is dumped at higher energy, which is a disadvantage. Even though there is no energy recovery in this design, the required RF power is similar to that in the oscillator design. Higher extraction efficiency requires a high quality electron beam and producing a high quality electron beam can be difficult.

The two proposed MW designs include approximate parameters which describe them. These parameters are being improved based on knowledge obtained through computer simulations and experiments. The parameters which resulted from the MW workshop for both the oscillator and amplifier designs are listed in Table 1. The two

Parameters	Oscillator	Amplifier
Beam Energy	100 MeV	100 MeV
Average Current	0.9 A	0.05 A
Extraction Efficiency	1%	20%
Undulator Type	Linear	Tapered
Undulator Parameter	1.0	1.0
Undulator Length	1 m	6 m
RF Power	6 MW	5 MW
Optical Power (IR)	1 MW	1 MW

Table 1. These are the MW ship self-defense parameters for the two proposed FEL designs.

designs have the same beam energy and they propagate the same wavelength radiation. They are different in most all other parameters. Typical FEL parameters are

listed throughout the theory chapter, Chapter 2. When comparing typical parameters with those for the MW designs in Table 1, the only real difference is found in the average current. The MW designs have a much higher average current, hence the resulting higher average power. Otherwise, the parameters listed are similar to any other FEL in the world.

IV. MW REGENERATIVE AMPLIFIER FEL

A. DESIGN PARAMETERS

In the previous chapter, two proposed MW FEL designs are discussed and the parameters for the two designs are listed in Table 1. These parameters resulted from the Navy's MW meeting held in September 1996. Improvements have been made to each of the designs. Much of the work to optimize the oscillator design was conducted by the FEL group at NPS through computer simulations, the results of which are in Ref. 17. The regenerative amplifier design has been proposed by LANL and Boeing with the analysis being performed at NPS. An analysis of the regenerative amplifier parameters is the topic of this chapter.

The design parameters for the MW regenerative amplifier (Figure 9) have evolved into two cases [Ref. 18]. Each is intended to provide the average optical power required to destroy an incoming anti-ship missile. The following parameters are common to both cases: the electron beam energy of 100 MeV, the normalized emittance of 6π mm-mrad, and the rms energy spread which is $\Delta\gamma/\gamma \approx 0.02\%$. In addition the electron beam energy (chosen to reach the 1 μm optical wavelength), the electron beam radius (0.17 mm), peak current (400 A), and pulse duration (20 ps) are common features. In each case, 4 m and 6 m long undulators are used in which the first half is uniform and the second half is tapered. These regenerative amplifiers will feedback on the order of 0.1% to 1% of the optical power and require an extraction efficiency of approximately 10% to 15%. These parameters are common to the two cases.

In case 1, the undulator parameter $K = 1.49$, the undulator period $\lambda_0 = 2.5$ cm, and the gap is 5.3 mm. The gap is the distance between the upper and lower portion of the undulator and affects the strength of the magnetic field at the midpoint of the gap. The optical beam radius in the uniform section is 0.3 mm and there are $N = 160$

undulator periods. The single pass gain is expected to be about 1000. Case 2 is more aggressive because it has a smaller gap size of 2.3 mm, a larger undulator parameter $K = 1.71$, and a shorter undulator period $\lambda_0 = 2.0$ cm. The optical beam radius in the uniform section is 0.25 mm and there are $N = 200$ undulator periods. This more aggressive design predicts single pass gain around 14,000. These parameters are listed in Table 2.

Parameters	Case 1	Case 2
Beam energy	100 MeV	100 MeV
Beam radius	0.17 mm	0.17 mm
Pulse duration	20 ps	20 ps
Peak current	400 A	400 A
K	1.49	1.71
λ_0	2.5 cm	2.0 cm
N	160	200
λ	1.045 μm	1.045 μm
Extraction efficiency	$\geq$ 15%	$\geq$ 15%
Single pass gain	~ 1000	~ 14,000

Table 2. Parameters for the MW regenerative amplifier designs developed at LANL.

B.   SIMULATIONS AND RESULTS

Computer simulations are used as an evaluation tool. One-dimensional simulations are used to describe a single pass of the optical wave through the undulator. The regenerative amplifier feeds back from 1% to 0.1% of the optical power, so we require the simulation achieve gains of $G \approx 100$ to $G \approx 1000$ in order to

34

operate in steady-state. The initial optical field a_0 is varied to achieve the desired gain. These simulations attempt to represent steady-state operation of the regenerative amplifier. The amount of taper in the undulator is determined by δ, the dimensionless artificial acceleration defined just above (36). The tapered undulator causes a shift in the phase velocity ν away from resonance for the untrapped electrons. The electrons inside the separatrix are trapped and therefore responsible for gain. The taper turns on at the most efficient point along the undulator in order to maximize extraction efficiency. These two parameters a_0 and δ are varied until the maximum possible extraction efficiency is obtained for gains of 100 and 10^3. The results for each case are given below.

1.   Case 1

The parameters for case 1, listed in Table 2, are used to derive dimensionless quantities. These dimensionless parameters are input into the computer simulation and the values of a_0 and δ are varied to optimize efficiency. The dimensionless current density is $j = 1500$ with $N = 160$ undulator periods. The electrons start on resonance, $\nu_0 = 0$, to maximize high gain consistent with Figure 5. The small Gaussian spread $\sigma_G = 0.4$ represents an energy spread of 0.02% as seen from (34). In this simulation, the taper $\delta = 70\pi$ turns on at $\tau \approx 0.5$. A large optical phase shift $\Delta\phi \approx 2\pi$, typical of a tapered undulator with high gain and strong fields, is similar to that of Figure 7. The best result for case 1 is final gain $G \approx 1100$ and extraction efficiency $\eta = 4\%$ given by $a_0 = 15$ and $\delta = 70\pi$ shown in Figure 10. Increasing a_0 tends to cause a decrease in gain while decreasing a_0 tends to increase gain. Increasing or decreasing δ primarily modifies the efficiency. Increasing δ beyond the optimum value tends to trap fewer electrons and reduce efficiency. Decreasing δ lower than the optimum value does not make full use of tapering and also reduces efficiency. Gain is defined as

$$G = \frac{|a_f|^2 - a_0^2}{a_0^2} \qquad (37)$$

where $|a_f|^2$ is the final field and a_0 is the initial optical field strength. Assuming large gain $G \gg 1$ gives

$$a_f \simeq a_0\sqrt{G} \qquad . \qquad (38)$$

In case 1, $a_f \simeq 500$ which means that if approximately 3% of the final optical field (0.1% of the power) is fed back and focussed at the beginning of the undulator, this system could operate in steady-state. While this feedback is reasonable, the extraction efficiency is substantially lower than the desired 15% indicating potential problems with this design.
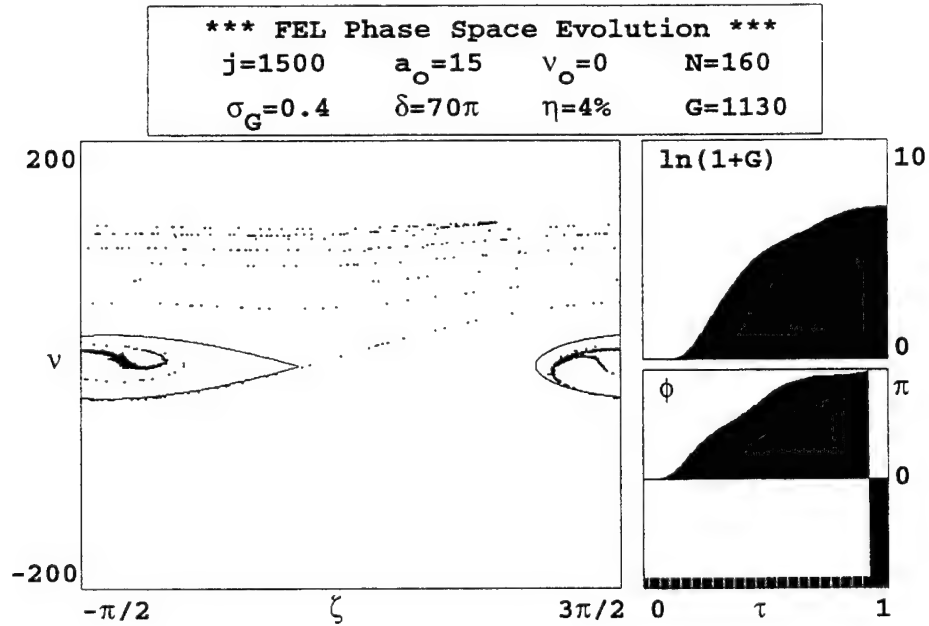

Figure 10. Phase space evolution for the regenerative amplifier, case 1, with a 4 meter undulator.

36

In an effort to obtain $\eta \approx 15\%$, it was mutually decided by LANL and the FEL group at NPS to increase the length of the undulator in this design from $L = 4$ m to $L = 6$ m. The dimensionless parameters are again calculated to be used in the simulation. The increased undulator length is responsible for the increased values of current density to $j = 5000$ with $N = 240$ undulator periods and energy spread $\sigma_G = 0.6$. High gain $j \gg \pi$, dictates $v_0 = 0$ once again. In this simulation, the taper turns on at $\tau \approx 0.3$ and the stronger taper causes a larger difference in phase velocity v between electrons which are trapped and those which are not. This difference is seen when comparing the v versus ζ portion of Figures 10 and 11. The optical phase shift also occurs earlier in Figure 11 than the phase shift of Figure 10. The same previous steps are taken and the best results are final gain $G \approx 1000$ and extraction efficiency reached $\eta = 8.6\%$. This result is represented in Figure 11 where $a_0 = 51$ and $\delta = 150\pi$. The maximum efficiency for any value of gain in Figure 11 is $\eta = 8.6\%$. As stated previously, increasing a_0 tends to cause a decrease in gain while
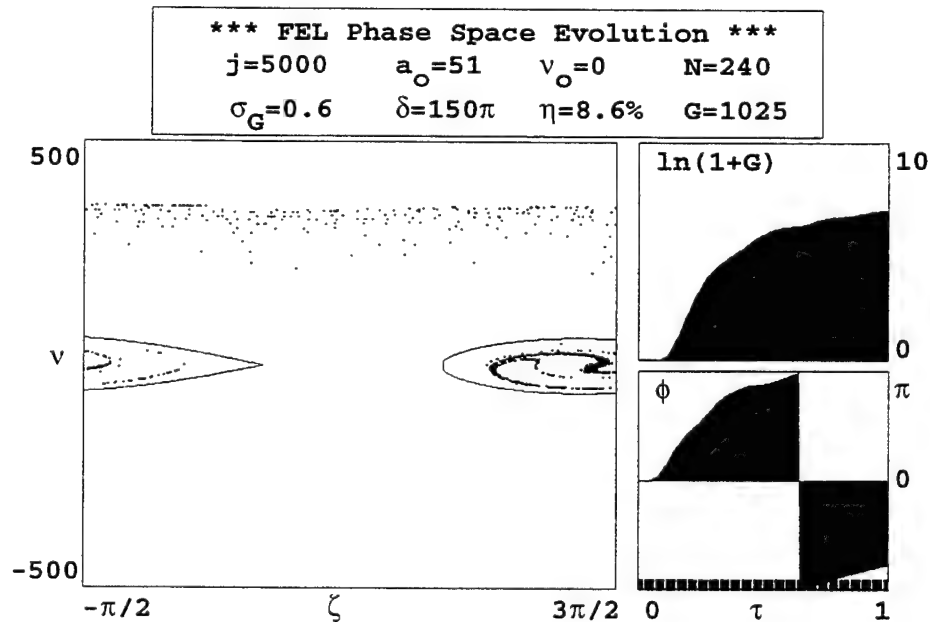

Figure 11. Phase space evolution for the regenerative amplifier, case 1, with a 6 meter undulator.

decreasing a_0 causes gain to rise. When δ is altered from its optimum value fewer electrons are trapped decreasing efficiency. The values of gain and initial optical field strength give $a_f \approx 1630$ so the required feedback is still approximately 3%. Even though gain is at the desired level, the extraction efficiency η is still less than the predicted 15%.

In another effort to reach 15% efficiency, the final gain is decreased from 1000 to 100. This is done by increasing both a_0 and δ. Increasing a_0 represents more feedback and stronger fields throughout the undulator, which leads to lower gain. It was expected that increasing a_0 would increase the trapping efficiency and therefore, the overall efficiency. The optimum case yielding the greatest efficiency is shown in Figure 12 where $a_0 = 122$ and $\delta = 122\pi$. The other parameters are the same as those in Figure 11. The taper starts at $\tau = 0.23$ which is similar to the taper start in the
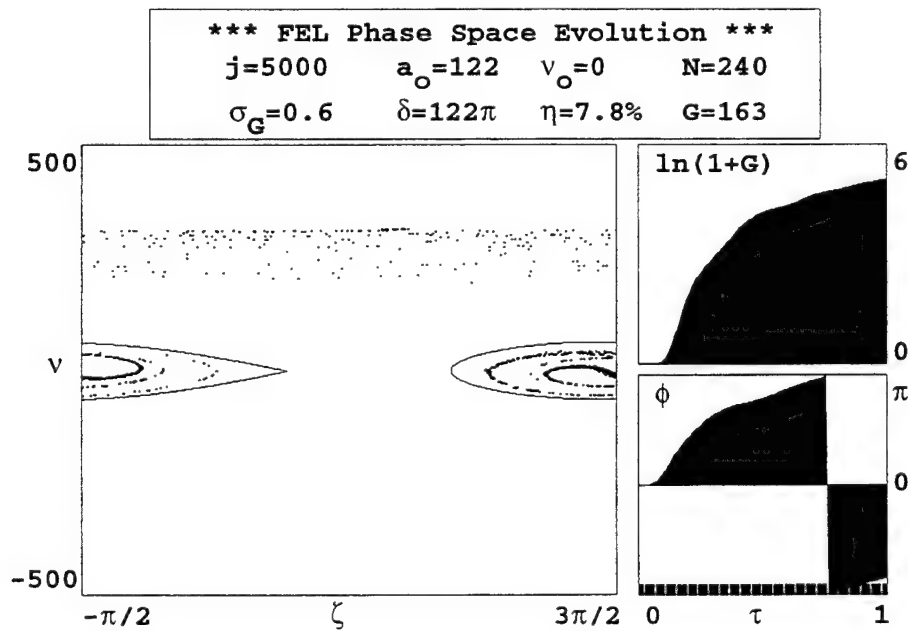

Figure 12. Phase space evolution for the regenerative amplifier, case 1, with a 6 meter undulator and gain $G = 100$.

previous figure. The result is $G = 163$ and $\eta = 7.8\%$, actually lower than the efficiency obtained when $G \geq 1000$. Increasing or decreasing either a_0 or δ has the same results as in the previous two trials. The reason for the decrease in efficiency here is that fewer electrons are trapped when the gain is lower. So, for case 1, the optimum results are represented by Figure 11 where $a_0 = 51$, $\delta = 150\pi$, $G = 1025$ and $\eta = 8.6\%$.

2. Case 2

The same procedures followed in case 1 are now followed for case 2. The parameters used to develop dimensionless quantities are taken from the beginning of this chapter and Table 2. The goals for this design are large gain of $G \geq 14,000$ and high efficiency of $\eta \approx 15\%$. In the simulation, the dimensionless current density $j = 3100$ with $N = 200$ undulator periods, and energy spread $\sigma_G = 0.5$. As in case 1, the maximum efficiency found in computer simulations is lower than predicted. The optimum values found are given in Figure 13 where $a_0 = 7$ and $\delta = 110\pi$. These results are $G = 15,400$ and $\eta = 4.7\%$. As in case 1, increasing a_0 tends to cause gain to decrease and decreasing a_0 results in increased gain. Changing δ from the optimum value 110π results in a decrease in efficiency. When δ is too high, fewer electrons are trapped reducing efficiency. When δ is too low, the taper is not being taken full advantage of which also reduces efficiency. The taper $\delta = 110\pi$ starts at $\tau \approx 0.5$. The calculated value for the final optical field $a_f \approx 870$ corresponds to about 1% of the optical field being fed back to the beginning of the undulator.

To obtain maximum efficiency, the goal of $G \geq 14,000$ is dropped. Varying both a_0 and δ, the maximum efficiency is found at $a_0 = 30$ and $\delta = 110\pi$. The result is given in Figure 14 where gain is $G = 1177$ and efficiency is $\eta = 6.6\%$. The taper in this simulation starts at $\tau = 0.36$. The increase in a_0 from 7 to 30 decreases gain so that the final field is $a_f \approx 1029$. If 3% of the field is fed back, this design could run in
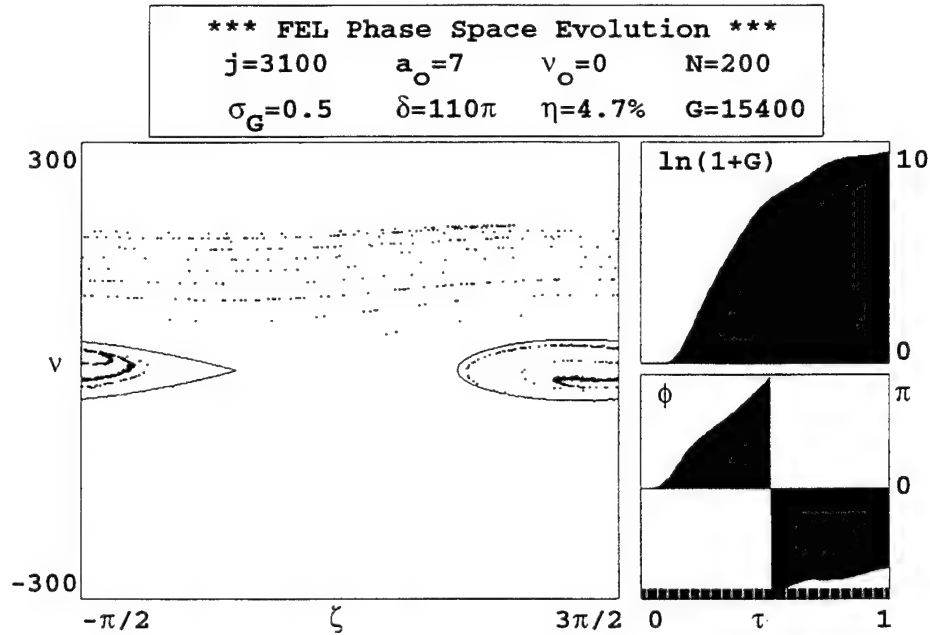
Figure 13. Phase space evolution for the regenerative amplifier, case 2, with a 4 meter undulator.

steady-state. However, this FEL does not produce the predicted extraction efficiency of 15%.

As in case 1, the undulator length is increased to 6 meters to try and obtain a higher efficiency. The longer undulator increases j to 10,400, increases the number of undulator periods to $N = 300$, and increases σ_G to 0.8. A stronger taper $\delta = 245\pi$ is used to obtain the maximum efficiency. The taper starts earlier at $\tau = 0.23$. The stronger taper causes a larger difference in phase velocity v between the trapped and untrapped electrons. The gain is also changed to $G \geq 1000$. The result of these simulations is shown in Figure 15 where $G = 1554$ and $\eta = 12.2\%$. The increased undulator length gives a higher value of the final optical field $a_f \approx 3150$. Therefore, with the same feedback of 3% of the field as in Figure 14, the value for the initial field

40

Figure 14. Phase space evolution for the regenerative amplifier, case 2, with a 4 meter undulator and no particular required gain.

is $a_0 = 80$. As with the previous two trials in this case, altering the optimum values of a_0 and δ has the same results on gain and efficiency as before. This case nearly achieves the required goal of 15% efficiency and is the most promising. The reason for higher efficiency here is that a higher percentage of electrons become trapped with $G \approx 1000$

As with case 1, the required gain is reduced from 1000 to 100 to try for higher efficiency. Again, the highest efficiency is found with $G \geq 1000$ instead of $G \geq 100$. The same parameters are used as in Figure 15 except for a_0 and δ. Also, the taper starts at $\tau = 0.17$ which is a little earlier than in the previous figure. The final gain is

$G = 139$ and the efficiency is $\eta = 10\%$ with initial field $a_0 = 243$ and taper $\delta = 175\pi$, as shown in Figure 16.
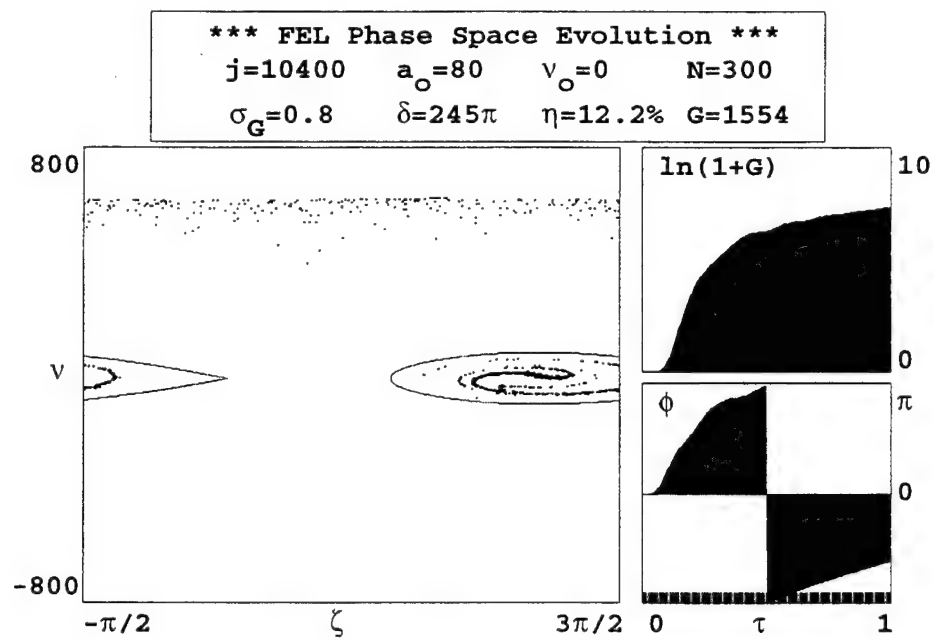
Figure 15. Phase space evolution for the regenerative amplifier, case 2, with a 6 meter undulator and required gain of 1000.

*** FEL Phase Space Evolution ***

$j=10400$ $a_o=243$ $\nu_o=0$ $N=300$
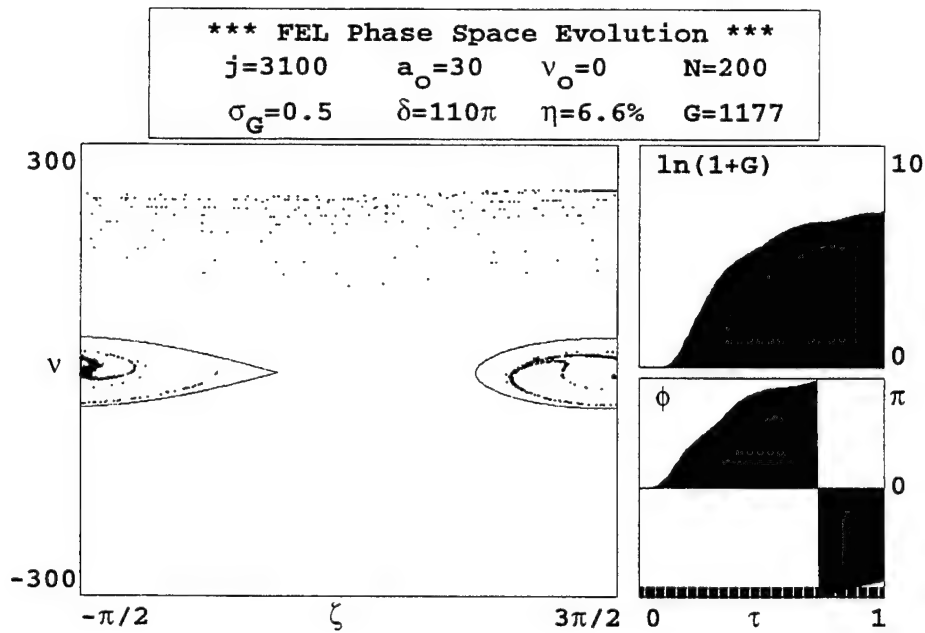
$\sigma_G=0.8$ $\delta=175\pi$ $\eta=10\%$ $G=139$
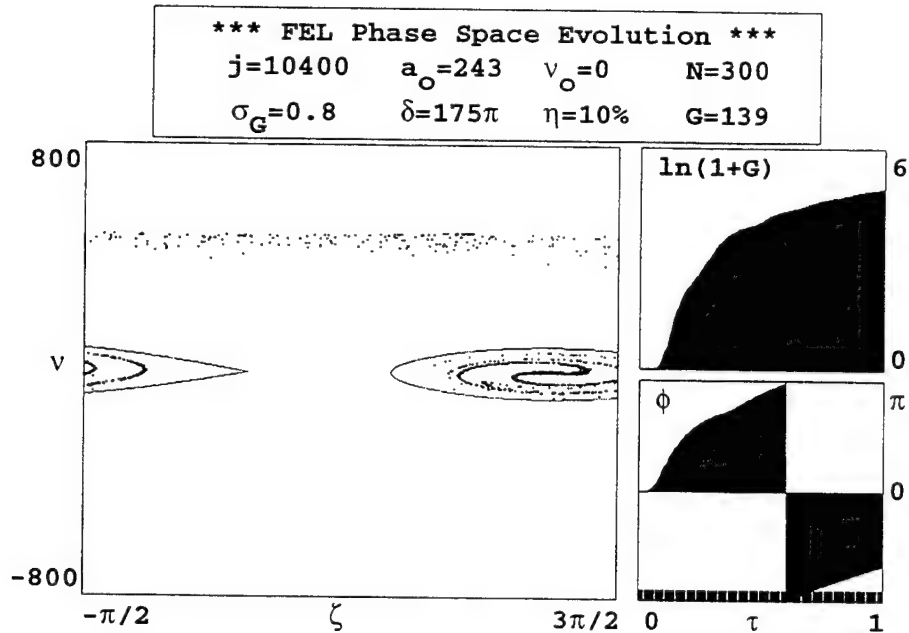
Figure 16. Phase space evolution for the regenerative amplifier, case 2, with a 6 meter undulator and required gain of 100.

C.   FUTURE ANALYSIS

One-dimensional computer simulations indicate that the two cases for the MW amplifier design will not yield the predicted extraction efficiency of $\eta \approx 15\%$. In the previous section, variations of the two cases gave values for the efficiency ranging from $\eta \approx 5\%$ to $\eta \approx 12\%$. It remains to be determined if 15% efficiency is actually necessary or if a somewhat smaller value is acceptable in the FEL weapon design. A lower efficiency would require higher beam current to achieve the same optical power.

The resulting values for gain and extraction efficiency obtained in the previous section may actually be over estimated, as they do not include the effect of diffraction of the optical beam. The definition for the filling factor given in Chapter II is $F = r_b^2/w_0^2$. The actual values used were $F \approx 0.3$ for case 1 and $F \approx 0.4$ for case 2, obtained from the original definition of the filling factor. If diffraction of the optical field occurs, then this definition of the filling factor is incorrect. When diffraction is present, the optical field will expand in area and decouple from the electron beam. From Chapter II, the dimensionless Rayleigh length is $z_0 = \pi w_0^2/(L\lambda)$. Case 1 gives a value of $z_0 \approx 0.07$ where the optical beam radius in the uniform section is 0.3 mm, the undulator length $L = 4$ meters, and the optical wavelength $\lambda = 1.045$ μm. For case 2 $z_0 \approx 0.05$. With such a short Rayleigh length, the optical beam would naturally expand in radius by a factor of ≈ 20 by the end of the undulator. The optical wavefront would effectively uncouple from the electron beam 10% to 20% along the undulator, greatly reducing gain and efficiency. This FEL design relies heavily on optical guiding, discussed at the end of Chapter II, to keep the optical beam focussed near the electron beam. Therefore, further analysis of diffraction is suggested.

V. ELECTRON BEAM TRANSPORT

A. REVIEW OF TRANSPORT WORKSHOP

In chapter III, the results of the Navy's ship self defense FEL workshop are discussed and two possible MW FEL designs are compared. The two designs are the oscillator design and the regenerative amplifier design which both have strengths and weaknesses. One characteristic specific to the oscillator design is energy recovery. While energy recovery is an advantage, it requires transporting a high energy bunched electron beam around four $180°$ bends. Imposing this bend on such a beam may cause coherent synchrotron radiation (CSR) to decrease beam quality. This effect has sparked Navy interest in CSR.

The Navy is not the only party interested in these results. Two other communities are commercial industry and high energy physics. A high-average-power FEL is of interest to commercial industry for use in surface processing of materials with ultra-violet (UV) light. This application is believed to have global markets totaling hundreds of billions of dollars [Ref. 19]. Energy recovery is a must for industrial applications because it drives down the cost of light produced by increasing overall system efficiency. It also eliminates the massive radiation management program required by a high energy beam dump. The application in the field of high energy physics is in particle beam colliders. Therefore, there are many reasons for gaining understanding of CSR's effect on beam quality.

The anticipated problem is that of a short electron bunch experiencing an acceleration and radiating coherently. The wavelength of the radiation is slightly greater than the bunch length, typically 1 mm to 1 cm. This radiation is termed "Coherent Synchrotron Radiation." The problem with CSR is that it causes an energy spread in the longitudinal direction and an emittance growth in the transverse direction which results in a degraded electron bunch. In a degraded bunch, the change in

energy causes electron trajectories to change. If severe enough, some high energy electrons could actually hit the vacuum cavity walls. Also, a degraded bunch could make energy recovery difficult since an energy spread decreases the effectiveness of beam transport in the recovery process. Although there are currently several theories, the physical processes involved in bending the beam are complex and not well understood. While the prediction of CSR dates back to around 1950, the effects of CSR on emittance have never been measured.

As a result of the Navy's interest in this phenomena, a prototype beam-bending problem was drafted by the FEL group at NPS. The problem included a micropulse common to most of the proposed MW designs presented at the TJNAF meeting. The prototype micropulses' peak current is 600 A with a full width, half maximum pulse duration of 3 picoseconds, and an electron beam energy of 100 MeV. The total bunch charge is 2.0 nC with a Gaussian longitudinal distribution. The nominal vacuum chamber width is 5 cm. The emittance and energy spread entering the bend are assumed perfect with zero spread. There is no specific bend design other than a continuous bend and one that is approximately achromatic and isochronous. What happens to this beam during a 180° bend with a bend radius of 2 meters?

This problem was sent to approximately 20 scientists who have some experience with CSR for possible analysis. Next, an electron beam transport workshop was held at NPS on March 6, 1997. The purpose of this workshop was to examine the analyses and discuss the possible effects of transporting a high-energy electron beam around a 180° bend. Along with the analyses, the comments made by the workshop speakers were discussed. The organizations represented during this meeting were the Navy's Directed Energy Office (SPAWAR), Los Alamos National Laboratory (LANL), Stanford Linear Accelerator Center (SLAC), Northrup Grumman, Thomas Jefferson National Accelerator Facility (TJNAF), and the Naval Postgraduate School (NPS).

B.   WORKSHOP CONCLUSIONS

As expected, there was not total agreement among the analyses performed by the workshop participants.   This stems from the many different CSR theories. However, a majority of the analyses gave similar CSR induced emittance growth. Overall, it is estimated that the CSR induced normalized rms emittance growth may be on the order of $\Delta\varepsilon_n \simeq 100\pi$'s mm-mrad. The goal for a typical infrared FEL is to be around $\varepsilon_n \simeq 20\pi$ mm-mrad, so a value of approximately 100π mm-mrad would result in a seriously degraded electron beam, and degraded FEL performance.

Since the effects of CSR on emittance have never been observed, a CSR experiment would help benchmark theories. Tests are planned at LANL in the summer of 1997, and at TJNAF in January of 1998. As a result, the FEL community is on the verge of being able to compare theoretical models with measured results of experiments.   One key in these observations is the actual accuracy of the emittance growth measurements.   Measuring emittance growth accurately is a difficult task. Therefore, small emittance growths can sometimes go undetected. For this reason, the participants of the workshop believe that there needs to be about a factor of two emittance growth in a system for actual detection to be feasible. In addition to the planned tests, workshop participants made a list of these and other possible experiments. Table 3 and Table 4 list the parameters for these possible CSR experiments. A simple analysis of these possible experiments is presented in the next section. As a result of this beam transport workshop, the Navy's Directed Energy Office has stated an interest in finding other organizations which would be able and willing to aid the Navy in funding a CSR experiment.

The parameters in Table 3 were obtained from each of the locations listed. There are two machines located at Los Alamos, one of which is an FEL. Both of these systems currently exist and are operational. Both the Princeton and Duke FELs are also operational. The TJNAF system is currently under construction and there are

Location	Beam Energy (MeV)	Peak Current (A)	Average Current	Normalized Emittance (π mm-mrad)	Energy Spread	Pulse Length (ps)	Beam Radius (fwhm)
LANL (AFEL)	17	300	0.5 A*	<8	<0.5%	6-15	0.5 mm
LANL (Compressor)	8	1500	10 nA	10	10%	0.7	200 µm-5 mm
Princeton	9-14	100	0.22 A*	10	0.2%	5	2 mm-5 mm
TJNAF (Chicane)	42	50	5 mA	13	0.5%	2.3	0.4 mm
(Recirculation Bend)	42	18	5 mA	14	0.5%	7	2.5 mm
Boeing	110	300	100 mA	15	0.3%	9	0.5 mm
Duke	44	40	0.18 A*	8-10	0.3%	2	0.2 mm
SLAC (Small Bend)	14,350	3400	95 nA	1.5	0.02%	0.23	0.03 mm
(Large Bend)	14,350	3400	95nA	1.5	0.1%	0.23	0.03 mm

* Average Current during macro-pulse.

Table 3. Electron beam parameters for possible CSR experiments.

two places in which emittance measurements will be made. The first is before and after a chicane, which is a bend used for bunch compression. The other place is before and after a 180° recirculation bend. There are two recirculation bends which allow this system to use the energy recovery technique. When looking for emittance growth in the recirculation bend, the undulator will be removed from the system so a strict CSR-induced emittance growth experiment, without undulator interaction, will be performed. Assembly of the Boeing FEL was stopped prior to commissioning trials due to lack of funding. The system at SLAC is still in the planning stages and is proposed to have two possible emittance growth measurement locations, each with

slightly different parameters. The beam radius is given as a full width, half maximum (fwhm) value.

Location	Undulator Periods N	Undulator Wavelength λ_0	Undulator Parameter K	Bend Radius/Arc
LANL (AFEL)	100	2 cm	1.0	-
LANL (Compressor)	-	-	-	0.25 m/45° (a)
Princeton	73	1.4 cm	0.2	0.2 m/90° (b)
TJNAF (Chicane)	40	2.7 cm	0.7	1 m/22° (c)
(Recirculation Bend)	-	-	-	1 m/180° (d)
Boeing	220	2.18 cm	1.31	42 cm/180° (e)
Duke	47	2.3 cm	1.0	43 cm/45° (f)
SLAC (Small Bend)	3330	3 cm	3.7	25 m/13.6° (g)
(Large Bend)	3330	3 cm	3.7	75 m/5.2° (h)

Table 4. Undulator and beam transport parameters for possible CSR experiments. (a) Chicane, achromatic. (b) Two 45° dipoles separated by two quads, forms 90° achromatic bend. (c) Four 22° dipoles for bunch compression and another identical chicane for bunch compression following the wiggler. (d) Two separate 180° recirculation bends, achromatic and isochronous. (e) Four 45° bends form a 180° bend, doubly achromatic and nearly isochronous. (f) Two 4-dipole chicanes, 11.25° per dipole, achromatic. (g) Four bend chicane, 3.4° per bend, achromatic. (h) Four bend chicane, 1.3° per bend, achromatic.

Table 4 lists parameters for the undulators and the bends of the possible CSR-induced emittance growth experiments. The FEL at Los Alamos (AFEL) is a straight

system which does not bend the electron beam before the undulator. However, as an FEL, the undulator does bend the electron beam repeatedly. It is not known whether this back and forth bending causes cancellation of the CSR effect or not. Therefore, one of the possible experiments is to measure any CSR wavelength radiation produced by the undulator. The compressor at Los Alamos is not an FEL, therefore there is no undulator. The TJNAF recirculation bend experiment, as previously stated, will be conducted without an undulator in the system. Therefore, no undulator parameters are listed for the recirculation bend experiment.

C.   ANALYSIS OF POSSIBLE EXPERIMENTS

A large CSR-induced emittance growth in a CSR experiment makes the effect easier to measure. Predicting this growth with computer simulations for each of the possible experiments can be a rather time-consuming task. Instead, a simplified analysis which examines steady-state CSR fields is conducted which enables the different experiments to be compared. This relative comparison is used to anticipate the experiments which may prove to be the most useful in learning about the CSR phenomena.

In this analysis, the final normalized emittance ε is given by

$$\varepsilon = \sqrt{\varepsilon_0^2 + (\Delta\varepsilon)^2} \tag{39}$$

where ε_0 is the initial normalized emittance of the beam at the bend entrance, and $\Delta\varepsilon$ is the change in normalized emittance due to CSR fields. The wavelength of the CSR emitted by the electron bunch is on the order of the bunch length itself. This coherent radiation wavelength is given by

$$\lambda \geq 2\pi\sigma \tag{40}$$

where σ is the rms bunch length [Ref. 20]. For example, a pulse length $\sigma = 0.5$ mm yields radiation $\lambda \geq \pi$ mm. Now, depending on the size of the vacuum chamber in

which the beam is transported, some or all of the CSR may be shielded by the walls of the cavity. For CSR fields to be unshielded by the vacuum chamber, the minimum chamber dimension should be much greater than

$$w^* = \left[R(\pi\sigma)^2 \right]^{1/3} \tag{41}$$

where w^* is the shielding dimension, and R is the bend radius. The normalized emittance growth $\Delta\varepsilon$ is estimated using

$$\Delta\varepsilon = 0.22\sigma_x \frac{I_p}{I_A} \left[\frac{R}{\sigma} \right]^{1/3} |\theta\sin\theta + \cos\theta - 1| \tag{42}$$

where σ_x is the transverse rms beam size averaged along the beam path, I_p is the peak current in the electron pulse, $I_A = 17,000$ A is the Alfven current, and θ is the bend angle of the beam path. This estimate of $\Delta\varepsilon$ assumes the electron bunch is rigid during the bend and the longitudinal CSR force is the main cause of emittance growth. Also, the transverse CSR force, which may contribute to emittance growth, is ignored. And, only single bunch effects are examined which means no effects of one bunch on another are included. [Ref. 21]

Table 5 and Table 6 lists the parameters required in this analysis. These parameters are constructed based on Tables 3 and 4. In Table 5, the AFEL at Los Alamos is not included since there are no transport bends in this system. The electron beam sizes are given as average values instead of a range of values and have been converted from fwhm to rms.

Table 6 lists parameters used to evaluate the different experiments. The values in the shielding chamber dimension column are calculated using (41). w is the actual minimum dimension of the vacuum chamber during the bend of each system. The right section of the table shows the estimated CSR-induced normalized emittance growth calculated using (42) and the final emittance calculated using (39). The percentage increase in emittance caused by CSR is also given. The three columns in

51

Location	I_p Peak Current	σ Bunch Length (rms)	σ_x Transverse rms beam size (avg)	R Bend radius	θ Bend angle
LANL (Compressor)	1500 A	0.09 mm	2.6 mm	0.25 m	45°
Princeton	100 A	0.64 mm	3.5 mm	0.2 m	90°
TJNAF (Chicane)	50 A	0.29 mm	0.4 mm	1.0 m	88°
(Recirculation Bend)	18 A	0.89 mm	2.5 mm	1.0 m	180°
Boeing	300 A	1.15 mm	0.5 mm	0.42 m	180°
Duke	40 A	0.26 mm	0.2 mm	0.43 m	45°
SLAC (Small Bend)	3400 A	0.03 mm	0.03 mm	25 m	13.6°
(Large Bend)	3400 A	0.03 mm	0.03 mm	75 m	5.2°

Table 5. Parameters for analysis of possible CSR experiments.

this right-hand section all assume that there is no CSR shielding by the vacuum chamber, $w \gg w^*$, which is not true for Duke and SLAC.

Comparing w and w^* indicates the experiments located at Duke and SLAC may shield some or all of the CSR as a result of their minimum vacuum pipe dimension since w is not much greater than w^* as required. On the basis of percentage emittance growth LANL, Princeton, Boeing, and SLAC have at least a factor of two emittance growth. Looking at all the parameters in Table 6 and remembering which FELs could support a CSR experiment in the near term, LANL Compressor and the Princeton FEL seem to be the best candidates.

Location	$w^\cdot$ Shielding chamber dimension	w Minimum chamber dimension	ε_0 Initial emittance (πmm-mrad)	$\Delta\varepsilon$ Emittance growth (πmm-mrad)	ε Final emittance (πmm-mrad)	$(\varepsilon/\varepsilon_0) - 1$ % Emittance growth
LANL (Compressor)	0.27 cm	2.0 cm	8	180	180.2	2150%
Princeton	0.93 cm	3.4 cm	10	18	21	110%
TJNAF (Chicane)	0.94 cm	5.0 cm	13	2	13.2	12%
(Recirculation Bend)	1.98 cm	5.0 cm	14	12	18	29%
Boeing	1.76 cm	7.0 cm	15	28	32	113%
Duke	0.66 cm	1.3 cm	10	0.3	10	0%
SLAC (Small Bend)	0.61 cm	0.2 cm	1.5	4	4.3	187%
(Large Bend)	0.87 cm	0.2 cm	1.5	0.7	1.7	13%

Table 6. Resulting parameters for analysis of possible CSR experiments.

D. PRINCETON FEL

One of the most readily available systems for a CSR experiment is the Compact Infrared FEL (CIRFEL) located at Princeton University. This FEL was developed by Northrop/Grumman Corporation and Princeton. The system is operational and encorporates a 90° bend prior to the undulator as part of the electron beam transport path. Parameters of this FEL are listed in Tables 3-6. Emittance could be measured at the entrance and exit to the bend with only slight modifications

to the system [Ref. 22]. The analysis in the previous section approximately predicts a factor of two emittance growth caused by CSR in the 90° bend making a CSR experiment feasible. Depending on the accuracy of those measurements, this could be the first exact measurement of the CSR effects on emittance. For these reasons, the CIRFEL seems to be a fruitful and possibly inexpensive tool for performing a CSR experiment.

Because of other priorities and funding issues, the CSR experiment has not already been performed. However, in an effort to further understand the CIRFEL, computer simulations of the FEL have been performed by Northrop/Grumman and the FEL group at NPS. Ongoing comparisons of these simulations hope to prove helpful in determining the limits of the CSR effect.

Since CIRFEL is operational, the gain of the system has been roughly measured. Comparison of the predicted and measured gain may give insight as to whether or not CSR induced emittance growth has occurred. Gain and emittance are coupled through beam quality. Large emittance gives poor beam quality which may cause lower gain. To calculate dimensionless parameters for the CIRFEL, some additional information about the electron beam is used. Northrop/Grumman reports that the full width, half maximum electron beam size in the vertical direction is 2 mm. In the horizontal direction the size of the beam varies. Horizontally, the beam is 5 mm at the undulator entrance, decreases to 2 mm at the center of the undulator, and is reported to be 10 mm at the undulator exit. To establish the effect of beam size on the FEL gain, the nominal sizes of 2 mm, 3 mm, and 4 mm are examined. Computer simulations at NPS yield final gain of 67%, 28%, and 20%, respectively, for the different beam sizes. Northrop/Grumman estimates gain around 30% which most closely corresponds to the NPS simulation with a beam size of 3 mm. The NPS simulations use initial emittance of 10π mm-mrad and emittance growth in the bend of $\Delta\varepsilon \approx 18\pi$ mm-mrad so the emittance seen at the entrance to the undulator is $\varepsilon \approx 21\pi$ mm-mrad. These values are taken from Table 6.

In conclusion, the analysis in this chapter predicts a factor of two CSR induced emittance growth and gain of approximately 30% for the CIRFEL. Because the actual initial emittance of the CIRFEL has not been measured, actual CSR induced emittance growth is not predicted. Measurements of gain and of emittance before and after the bend will be an excellent benchmark for this analysis and is recommended. Performing this experiment will help the Navy decide if the MW oscillator FEL design is a real possibility or if energy recovery is risky due to CSR.

LIST OF REFERENCES

1. Murphy, J. B. et. al. in: *Laser Handbook,* Vol. 6, Chapter 2, eds W. B. Colson, C. Pellegrini, and A. Renieri, North-Holland, 1990.

2. Colson, W. B. in: *Laser Handbook,* Vol. 6, Chapter 5, Section 1, eds W. B. Colson, C. Pellegrini, and A. Renieri, North-Holland, 1990.

3. Colson, W. B., Ph.D. Thesis, Stanford University, 1977.

4. Jackson, J. D., *Classical Electrodynamics,* 2nd ed., John Wiley & Sons, Inc., 1975.

5. Colson, W. B. in: *Laser Handbook,* Vol. 6, Chapter 5, Section 5, eds W. B. Colson, C. Pellegrini, and A. Renieri, North-Holland, 1990.

6. Colson, W. B. in: *Laser Handbook,* Vol. 6, Chapter 5, Section 19, eds W. B. Colson, C. Pellegrini, and A. Renieri, North-Holland, 1990.

7. Colson, W. B. in: *Laser Handbook,* Vol. 6, Chapter 5, Section 7, Page 137, eds W. B. Colson, C. Pellegrini, and A. Renieri, North-Holland, 1990.

8. Colson, W. B. in: *Laser Handbook,* Vol. 6, Chapter 5, Section 8, Page 143, eds W. B. Colson, C. Pellegrini, and A. Renieri, North-Holland, 1990.

9. Colson, W. B. in: *Laser Handbook,* Vol. 6, Chapter 5, Section 10, eds W. B. Colson, C. Pellegrini, and A. Renieri, North-Holland, 1990.

10. Steenbergen, A. van in: *Laser Handbook,* Vol. 6, Chapter 12, eds W. B. Colson, C. Pellegrini, and A. Renieri, North-Holland, 1990.

11. Colson, W. B. in: *Laser Handbook,* Vol. 6, Chapter 5, Section 11, eds W. B. Colson, C. Pellegrini, and A. Renieri, North-Holland, 1990.

12. Colson, W. B. in: *Laser Handbook,* Vol. 6, Chapter 5, Section 12.1, eds W. B. Colson, C. Pellegrini, and A. Renieri, North-Holland, 1990.

13. Colson, W. B. in: *Laser Handbook,* Vol. 6, Chapter 5, Section 20, eds W. B. Colson, C. Pellegrini, and A. Renieri, North-Holland, 1990.

14. Anderson, E. J., Master's Thesis, Naval Postgraduate School, 1996.

15. Notes of Navy MW-Class SSD FEL Concepts Workshop, Thomas Jefferson National Accelerator Facility, 1996.

16. Small, D. W., Restivo, R. A., Wong, R. K., and Colson, W. B., "Free Electron Lasers with Short Rayleigh Length," *Proceedings of the 18th International FEL Conference,* Rome, Italy, 1996.

17. Small, D. W., Ph.D. Thesis, Naval Postgraduate School, 1997.

18. Sheffield, R. L., Los Alamos National Laboratory, private communication, 1997.

19 The Laser Processing Consortium, "High-Power Ultraviolet and Infrared Free Electron Laser for Industrial Processing," Proposal, 1994.

20. Dowell, D. H., O'Shea, P. G., "Coherent Synchrotron Radiation Induced Emittance Growth in a Chicane Buncher," *Proceedings of the 1997 Particle Accelerator Conference,* Vancouver, Canada, 1997.

21 Bisognano, J. J., Bohn, C. L., Li, R., "Transient Coherent Synchrotron Radiation in Magnetic Bending Systems," Jefferson Lab preprint, 1996.

22. Bruhwiler, D. L., Northrup Grumman Corporation, private communication, 1997.

INITIAL DISTRIBUTION LIST

1. Defense Technical Information Center   2
    8725 John J. Kingman Road, Ste 0944
    Fort Belvoir, VA 22060-6218

2. Dudley Knox Library   2
    Naval Postgraduate School
    411 Dyer Rd.
    Monterey, CA 93943-5101

3. Professor William B. Colson, PH/Cw   2
    Department of Physics
    Naval Postgraduate School
    Monterey, CA 93943-5000

4. Mr. John Albertine   1
    Code 332, Division Director
    Directed Energy Division
    Space and Naval Warfare Systems Command
    2541 Crystal Dr.
    Arlington, VA 22245-5200

5. Dr. David Bruhwiler   1
    Northrop Grumman Corporation
    4 Independence Way
    Princeton, NJ 08540

6. Dr. Alan Todd   1
    Northrop Grumman Corporation
    4 Independence Way
    Princeton, NJ 08540

7. Dr. Court Bohn 1
    Accelerator Division
    Jefferson Laboratory
    12000 Jefferson Avenue
    Newport News, VA 23606

8. Dr. Fred Dylla 1
    Jefferson Laboratory
    MS 12A
    12000 Jefferson Avenue
    Newport News, VA 23606

9. Dr. George Neil 1
    Jefferson Laboratory
    MS 12A
    12000 Jefferson Avenue
    Newport News, VA 23606

10. Dr. Patrick O'Shea 1
    Duke University
    Box 90319
    Durham, NC 27708

11. Dr. Rich Sheffield 1
    Los Alamos National Laboratory
    MS-H851
    Los Alamos, NM 87545

12. Troy McQueen 1
    RR 2 Box 2051
    Columbus, TX 78934